Glassy slowing of stripe modulation in $(La,Eu,Nd)_{2-x}(Sr,Ba)_xCuO_4$: A ^{63}Cu and ^{139}La NQR study down to 350 mK

A. W. Hunt, P. M. Singer, A. F. Cederström, and T. Imai
Department of Physics and Center for Materials Science and Engineering, Massachusetts Institute of Technology, Cambridge, Massachusetts 02139

(Received 22 November 2000; published 13 September 2001)

^{63}Cu and ^{139}La nuclear quadrupole resonance and Zeeman perturbed nuclear magnetic resonance experiments are performed on the striped phase of the high-temperature superconductors $La_{2-x}Ba_xCuO_4$ and $La_{2-x-y}(Nd,Eu)_ySr_xCuO_4$. The first goal of the present study is to utilize the fact that ordered Cu magnetic moments exert a static hyperfine field on the ^{63}Cu and ^{139}La nuclei to deduce the charge density and ordered moment within the CuO_2 planes. A hyperfine-broadened nuclear quadrupole resonance (NQR) line shape is observed in both $La_{2-x}Ba_xCuO_4$ and $La_{1.80-x}Eu_{0.20}Sr_xCuO_4$ for $x\approx\frac{1}{8}$. Detailed numerical analysis of the ^{63}Cu NQR line shape establishes that widely accepted models of periodic sinusoidal or square-well-shaped modulations of spin density waves with maximum moment $\sim 0.3\ \mu_B$, as inferred from elastic neutron scattering and muon spin rotation (μSR) measurements, *cannot* account for the NQR line shape unless we assume a relatively small ordered moment $\sim 0.15\ \mu_B$ with a comparably large distribution. The second goal of the present work is to establish the temperature dependence of the fluctuation frequency scale of stripes. We find that the fraction of missing ^{63}Cu NQR intensity below charge ordering temperature T_{charge} accurately tracks the temperature dependence of the charge order parameter as measured by scattering methods. By fitting a *single* model to the temperature dependences of the wipeout fraction $F(T)$ for ^{63}Cu and ^{139}La NQR, the spin order parameter measured by elastic neutron scattering, and the μSR data, we deduce the spatial distribution of the spin fluctuation frequency scale Γ and its temperature dependence. These results indicate that as soon as the charge dynamics slow down, the spin fluctuations begin to slow dramatically with spin stiffness $2\pi\rho_s^{eff}\sim 200$ K. By extending the analysis to other hole concentrations, we demonstrate a qualitative difference in the spatial variation of electronic states induced by slowing the charge dynamics above and below $x=\frac{1}{8}$.

DOI: 10.1103/PhysRevB.64.134525 PACS number(s): 74.72.−h, 76.60.−k

I. INTRODUCTION

The electronic phase diagram of high-T_c cuprates involves a number of different phases and crossovers, including an undoped antiferromagnetic phase (Néel state), an insulator-metal crossover, a spin-glass phase, a pseudogap phase, and an overdoped metallic regime, in addition to the superconducting phase. The complexity of the phase diagram makes it difficult to identify the superconducting mechanism. Some of the aformentioned phases and crossovers may be irrelevant to the superconducting mechanism, while others may prove to be critical.[1] Further experimental efforts are necessary to elucidate the properties of each phase, as well as the nature of transitions and crossovers between adjacent phases.

A relatively new addition to the already complex electronic phase diagram of high-T_c cuprates is the so-called *stripe phase* near the magic hole concentration $x\approx\frac{1}{8}$. It has been demonstrated by elastic neutron scattering experiments on Nd-codoped $La_{2-x}Sr_xCuO_4$ by Tranquada *et al.* that doped holes microscopically phase segregate into hole rivers forming a charge density wave (CDW).[2] The hole rivers become antiphase boundaries between hole-poor segments in which Cu spins form a short-range spin density wave (SDW) order. Recent measurements based on neutron scattering,[3–9] nuclear quadrupole resonance (NQR),[10–14] electron spin resonance (ESR),[15,16] x-ray scattering,[17,18] charge transport,[19–24] photoemission spectroscopy,[25,26] and muon spin rotation (μSR),[27–32] detect experimental signatures of the stripe instabilites in the underdoped regime.

A major difficulty in applying NMR techniques to investigate the stripe phase of high-T_c cuprates is in the *glassy* nature of the slowing down of stripes that is observed for most striped cuprates [9,29] [one exception being $La_2CuO_{4+\delta}$ Refs. 6 and 32]. Unlike ordinary second-order phase transitions, the slowing of stripe fluctuations is very gradual and inhomogeneous. This means that the experimental signature of stripe freezing appears at different temperatures depending on the characteristic frequency of the experimental probe. If one uses a probe with a lower-frequency scale, the stripe anomaly takes place at a lower temperature. Furthermore, the glassy freezing of the stripes does not show typical signatures of the phase transitions observed by NMR, such as a divergence of NMR spin-lattice and spin-spin relaxation rates $1/T_1$ and $1/T_2$ at the onset of freezing. That explains why earlier NMR studies of underdoped high-T_c cuprates carried out before the discovery of stripes by Tranquada *et al.* by neutron scattering failed to capture the various signatures of stripe instabilities in a convincing manner, even though there are some results that seem, retrospectively, consistent with stripe anomalies.[33–40]

Very recently, we demonstrated that the slowing of stripes in $La_{2-x}Sr_xCuO_4$ with and without Nd or Eu rare-earth codoping and in $La_{1.875}Ba_{0.125}CuO_4$ can be easily captured by measuring the anomalous reduction (i.e., *wipeout*) of the ^{63}Cu NQR intensity.[10,11]

In our earlier publications,[10,11] we left some important issues unexplored. First, if stripes keep slowing down with decreasing temperature, what kind of spin and charge density modulation does the stripe phase exhibit in the ground state *at NMR and NQR time scales*? Second, what is the spatial distribution of the stripe fluctuation frequency? Third, how does the hole concentration affect the slowing of stripes? In order to address these issues, we now report a more detailed ^{63}Cu and ^{139}La NQR study of $La_{1.875}Ba_{0.125}CuO_4$ and (Nd, Eu) codoped $La_{2-x}Sr_xCuO_4$ near the magic hole concentration $x \approx \frac{1}{8}$ down to 350 mK. In Sec. III, we report Zeeman-preturbed ^{63}Cu and ^{139}La NQR line shapes including detailed numerical simulations. Our preliminary line shape measurements on ^{63}Cu-isotope-enriched samples conducted for our earlier publication[10] did not reveal any noticeable structures down to 1.7 K other than a single peak, in agreement with an earlier finding by Tou *et al.* reported for a ^{63,65}Cu mixed-isotope sample.[35] This made us suspect that stripes are still fluctuating quickly enough relative to NQR time scales to *motionally narrow*[41,42] the line shapes at 1.7 K. Accordingly, we developed a top-loading ^{3}He NMR system to conduct NQR line shape measurements in a broad frequency range down to 350 mK in the hope that any stripe excitations with energy $\Delta E/k_B \sim 1$ K or higher would be suppressed. However, our results at 350 mK demonstrate that a *periodic* spatial modulation of spin and charge density hardly exists at NQR time scales even at 350 mK. This is in remarkable contrast with elastic neutron, x-ray, and μSR measurements that sucessfully detect short-range spin and charge order *at time scales that are three to seven orders of magnitude faster than NQR measurements*. Our NQR results suggest that the short-range stripe order is highly disordered or that extremely slow dynamic fluctuations persist even at 350 mK or probably both. In Sec. IV, we analyze the distribution of ^{139}La nuclear relaxation $^{139}1/T_1$ and demonstrate that below charge ordering, glassy slowing of the Cu spins fluctuations sets in and results in a large spatial distribution of $^{139}1/T_1$. We also analyze the wipeout of ^{63}Cu and ^{139}La. We employ the renormalized classical scaling in the nonlinear σ model to fit the entire set of existing data with a small spin stiffness ($2\pi\rho_s^{eff} \lesssim 200$ K) which is reduced due to slowed charge dynamics. This analysis accounts for the temperature dependences of not only the ^{63}Cu NQR wipeout, but also the ^{139}La NQR wipeout, the order parameter of spin stripes measured by elastic neutron scattering, the μSR asymmetry, and the recovery of both ^{63}Cu and ^{139}La NQR intensity, all within a single framework. From the analysis, we estimate the spatial distribution of stripe fluctuations as a function of temperature. We find that below T_{charge} the glassy slowing down of stripes results in three orders of magnitude distribution in fluctuation frequencies in agreement with our analysis of $^{139}1/T_1$. This is in contrast to the well-known neutron results in the normal metallic state of $La_{2-x}Sr_xCuO_4$, where the spin fluctuation energy scale $h\Gamma$ is well defined by a single value on the order of k_BT and that $h\Gamma$ varies roughly in proportion to T as originally discovered by Keimer *et al.*[43] (called ω/T *scaling*[43,44] or *quantum critical behavior*[45]). In Sec. V, we extend the analysis to deduce a diagram of temperature versus stripe fluctuation frequency for various hole concentrations.

II. EXPERIMENT

All of the single-phase and polycrystalline samples of $La_{2-x-y}(Eu,Nd)_y(Ba,Sr)_xCuO_4$ used in this study were prepared using conventional solid-state procedures. We mixed predried La_2O_3 (99.99%), Eu_2O_3 (99.99%), Nd_2O_3 (99.99%), $BaCO_3$ (99.95%), $SrCO_3$ (99.99%), and CuO (99.995%) with correct nominal compositions, and ground by hand with an agate mortar and pestle until an intimate mixture is obtained. To make complicated line shape analysis feasible, some samples were enriched with either ^{63}Cu or ^{65}Cu isotopes. This first grinding usually consumed 40–60 min for the 1–4 g of powder that we prepare. A prereaction was carried out for 20 h in a box furnace at 850 °C followed by repeated regrindings and sinterings (also 20 h) at temperatures between 950 and 1000 °C. Finally the samples were pelletized and high-temperature annealed in flowing O_2 gas at 1100–1150 °C for 24–48 h before a slow and controlled cooling cycle that includes low-temperature annealing at 800 °C (24 h) and 500 °C (24 h). By using a large number of grindings (typically 5–8), we acheived homogenous, high-quality polycrystalline samples. The powder x-ray spectra revealed that all samples were single phased. The measured lattice parameters showed systematic variation through the sample families as a function of hole concentration, revealing the room-temperature orthorhombic-to-tetragonal structural transition, and were well within the range of previously published data.[46] To further characterize the prepared samples, magnetization measurements were performed with a superconducting quantum interference device (SQUID) magnetometer at a field of 10 Oe. All superconducting samples showed a clear diamagnetic response, and T_c and the volume fraction were consistent with previous measurements.[47] Nonsuperconducting samples showed no Meissner shielding down to 5 K.

All nuclear resonance data were taken with a homemade, phase-coherent pulsed NMR spectrometer using the standard $\pi/2$-τ-π pulse sequence with a typical pulse separation time $\tau = 12$ μs. For measurements at and above 1.7 K we used a commercial cryostat and measured temperature with calibrated Cernox and carbon-glass resistors. In order to conduct Zeeman-perturbed NQR measurements in zero applied field down to 350 mK, we developed a top-loading NMR system utilizing a commercial single-shot ^{3}He refrigerator. In those cases, temperature was measured via a calibrated ruthenium oxide temperature sensor.

III. ZEEMAN-PERTURBED NQR LINE SHAPE

A. Principles of Zeeman-perturbed NQR

In the Néel-ordered state of the undoped parent compounds of high-T_c cuprates, Zeeman perturbed NQR has been sucessfully utilized to measure the sublattice magnetization $\langle S_i \rangle$ and its temperature dependence. In antiferromagnets below the Néel temperature T_N, the nuclear resonance frequency f_i of the ith site depends on $\langle H_i \rangle$, the static com-

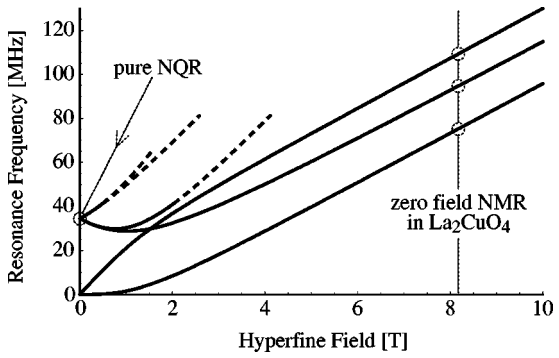

FIG. 1. Plot of ^{63}Cu NQR ($I=\frac{3}{2}$) transition frequencies as a function of hyperfine field in the ab plane with an axially symmetric quadrupole tensor $\nu_Q^c=34.5$ MHz. This chart is applicable for the case of ^{63}Cu resonance in $La_{1.875}Ba_{0.125}CuO_4$. The dashed lines mark transitions that occur with very low probability. The intersects of three solid curves and the dotted vertical line at $H=8.2$ T correspond to three zero-field Cu NMR lines observed for La_2CuO_4 by Tsuda *et al.* (Ref. 50) (to be rigorous, $\nu_Q^c=31.9$ MHz at 1.3 K in La_2CuO_4).

ponent of hyperfine magnetic field at that site. Typically, $\langle H_i\rangle$ originates from the hyperfine coupling A^{ii} with the ordered magnetic moment $\langle S_i\rangle$ at the same site and from the transferred hyperfine coupling A^{ij} with the ordered magnetic moment $\langle S_j\rangle$ at the nearest-neighbor sites. Since the hyperfine coupling constants can be determined based on NMR measurements in the paramagnetic state above T_N, one can utilize the nuclear resonance frequency f_i to measure the hyperfine magnetic field $\langle H_i\rangle$ and, hence, the sublattice magnetization $\langle S_i\rangle$.[48,49] This technique has been employed successfully in the Néel state of several undoped parent compounds of high-T_c cuprates.[50–53] In the case of undoped La_2CuO_4 ($T_N=325$ K), Tsuda *et al.*[50] find three peaks corresponding to the transitions $|I_z=+\frac{3}{2}\rangle\leftrightarrow|+\frac{1}{2}\rangle$, $|+\frac{1}{2}\rangle\leftrightarrow|-\frac{1}{2}\rangle$, and $|-\frac{1}{2}\rangle\leftrightarrow|-\frac{3}{2}\rangle$ for each of the ^{63}Cu and ^{65}Cu isotopes (both have nuclear spin $I=\frac{3}{2}$). Defining $A_x\equiv A^{ii}$ as the x component of the on-site hyperfine coupling constant and $B\equiv A^{ij}$ as the isotropic supertransferred hyperfine coupling constant from the four nearest-neighbor Cu sites,[54] the hyperfine magnetic field at the nuclear site i can be written as

$$\langle H_i\rangle = A_x\langle S_i\rangle + B\sum_{j\in nn}\langle S_j\rangle, \tag{1}$$

where the sum is taken over the four nearest neighbors. We also use the fact that the ordered Cu moments lie within the ab plane.[55] For the present case of a two-dimensional square-lattice antiferromagnet, $\langle S_i\rangle=-\langle S_j\rangle$ for nearest neighbors i and j. Then Eq. (1) simplifies to

$$\langle H_i\rangle = (A_x-4B)\langle S_i\rangle. \tag{2}$$

From the analysis of the three transitions of ^{63}Cu zero-field NMR (see Fig. 1), Tsuda *et al.* find the internal field at the Cu nucleus to be $\langle H_i\rangle=8.2$ T in La_2CuO_4.[50] On the other hand, the hyperfine coupling constants are known to be $A_x=38$ kOe/μ_B and $B=42$ kOe/μ_B.[56,54] Together, these values imply an effective moment of $|\langle S_i\rangle|=|\langle S_j\rangle|\approx 0.63\mu_B$, in accordance with previous results of muon spin precession measurements, which indicate a moment of $\sim 0.58\mu_B$.[57] Additionally, the frequency splitting between two satellite transitions $|I_z=+\frac{3}{2}\rangle\leftrightarrow|+\frac{1}{2}\rangle$ and $|-\frac{1}{2}\rangle\leftrightarrow|-\frac{3}{2}\rangle$ provides information regarding the nuclear quadrupole interaction tensor, which reflects the second derivative of the electrostatic Coulomb potential at the Cu sites.[41,42] The splitting data may be used, in principle, to obtain information regarding the charge state of the observed nuclei.[50,51]

If well-defined static charge and magnetic order exist in the striped materials, we would expect similar, highly structured resonance line shapes arising from each unique Cu site, from which we could gain insight into the spin state from the measured hyperfine magnetic field H_i and the charge state from the nuclear quadrupole interaction tensor ν_Q. Contrary to these expectations, we observed no evidence for well-defined periodic spin and charge density modulations even at 350 mK, as will be described in the following sections.

B. ^{63}Cu NQR and NMR spectra in $La_{1.875}Ba_{0.125}CuO_4$

In 1991, magnetic order was discovered in a $x=\frac{1}{8}$ doped sample of $La_{2-x}Ba_xCuO_4$ using μSR by Luke *et al.*[27] The next year, Tou *et al.* reported anomalous broadening of the low-temperature ^{63,65}Cu NQR spectra, consistent with Zeeman-perturbed NQR.[35] Here we provide a comprehensive understanding of the low-temperature Cu resonance line shape in light of the progress that has been made in the field of stripe physics. As demonstrated earlier by Hunt *et al.*[10] and Singer *et al.*,[11] most of the NQR response of Ba-, Nd-, and Eu-doped materials is semiquantitatively identical for $x\approx\frac{1}{8}$. In the following, we focus our discussion of the NQR line shapes on the $La_{1.875}Ba_{0.125}CuO_4$ sample. The Nd-doped materials are ill suited for Zeeman-perturbed NQR measurements at low temperatures due to the large Nd^{3+} local moments that make the relaxation rates too fast, and the Eu-doped samples show extra NQR peaks as discussed in Sec. III F.

Selected ^{63}Cu NQR line shapes for ^{63}Cu-isotope-enriched $La_{1.875}Ba_{0.125}CuO_4$ are shown in Fig. 2. At high temperatures we observe the well-known A and B NQR lines.[58] The relative intensity of the B line is the same as the doped concentration x of the impurity ions Ba^{2+} and Sr^{2+}, over a broad concentration range $0.02\leqslant x\leqslant 0.30$.[59,60] Furthermore, the B line is known to be observable even at elevated temperatures as high as 800 K.[60] Accordingly, it is unlikely that the B line originates from electronic effects such as phase separation or stripes. The most likely scenario is that the B line arises from Cu sites directly across the apical O from the doped Ba position and the lattice contribution to the electric field gradient is different due to the presence of a Ba^{2+} ion rather than La^{3+}. Needless to say, this line assignment of the B line does not exclude the possibility that the B site has a somewhat different local electronic state as compared to the surrounding A sites. In fact, $^{63}1/T_1$ is known to be somewhat smaller for the B site as shown by Yoshimura *et al.*[58] In Fig. 7 we also show that Eu codoping results in a new structure at the low-frequency side of the A line. We attribute this structure to the Cu site sitting across the apical O from the Eu^{3+} ions.

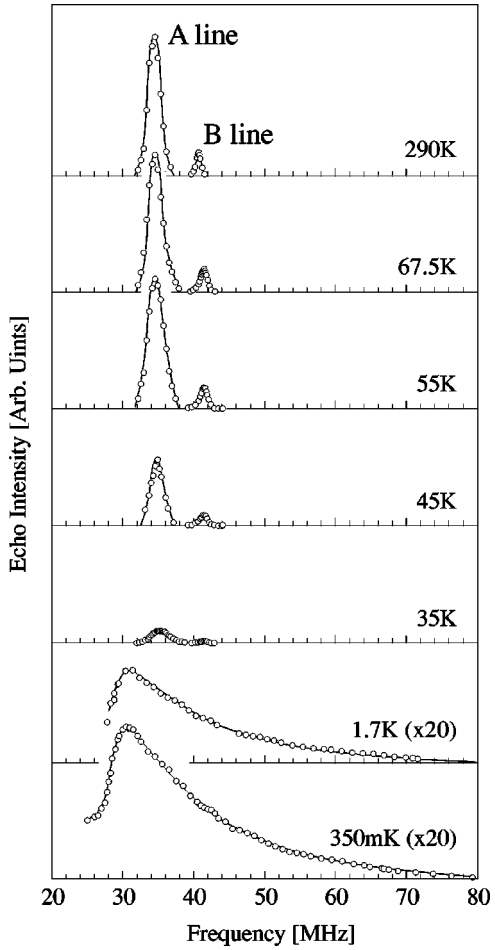

FIG. 2. ^{63}Cu NQR line shapes of a ^{63}Cu-isotope-enriched $La_{1.875}Ba_{0.125}CuO_4$ sample at selected temperatures, including pure NQR from 290 K down to 70 K, partially ''wiped-out'' NQR at 55 K, 45 K, and 35 K, and Zeeman-perturbed NQR at 1.7 K and 350 mK. ^{63}Cu resonance continues below $\sim$25 MHz in the Zeeman-pertubed case, but is obscured by the ^{139}La NQR $|I_z=\pm\frac{7}{2}\rangle\leftrightarrow|\pm\frac{5}{2}\rangle$ transition peaked near 18 MHz which is more than an order of magnitude stronger in intensity (not shown). Note the scale multipliers when comparing magnitudes. The solid curves are guides for the eye. The 1.7 K and 350 mK curves are identical except for overall magnitude.

The temperature dependence of the integrated ^{63}Cu NQR intensity is presented in Fig. 3. Since the occupation probability of nuclear spin levels is determined by the Boltzmann factor, the bare NQR intensity is inversely proportional to temperature *T*. Accordingly, we multiply the bare NQR intensity by *T* to correct for the Boltzmann factor. We also calibrate the intensity of the observable NQR signal by extrapolating the observed spin-echo decay to $2\tau=0$. The NQR intensity thus deduced corresponds to the number of nuclear spins whose resonance conditions are well defined and whose relaxation times $^{63}T_1$ and $^{63}T_2$ are long enough to be observed experimentally within the time domain of pulsed NQR measurements, $\tau_{NQR}\sim 20$ μsec. The missing signal intensity arises because at least one of these conditions is violated for the lost signal.[10,11] We note that these are standard procedures that have also been applied to the NMR investi-

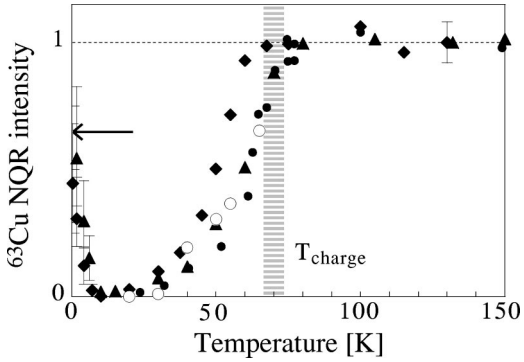

FIG. 3. Integrated ^{63}Cu NQR intensity above 25 MHz for $La_{1.875}Ba_{0.125}CuO_4$ (♦), $La_{1.68}Eu_{0.20}Sr_{0.12}CuO_4$ (▲), and $La_{1.48}Nd_{0.40}Sr_{0.12}CuO_4$ (●) scaled for the Boltzmann factor and T_2 spin-echo decay. In addition, we plot the charge order parameter (○) deduced from neutron scattering on the Nd-codoped material (Ref. 2). Within the broadened hyperfine field model in Fig. 5(f), the maximum recovery of signal above 25 MHz is expected to be 61%, as indicated by the arrow.

gation of the SDW state in electron-doped $Nd_{2-x}Ce_xCuO_4$ by Kambe *et al.*[61] Between room temperature and 70 K the lines retain constant intensity, as expected, because the number of ^{63}Cu nuclear spins detected by NQR measurements is unchanged. The peak frequency $\nu_Q(A)$ displays only a small temperature dependence down to $T_{charge}\approx 70$ K as shown in Fig. 4. The weak temperature dependence of $\nu_Q(A)$ down to 70 K can be accounted for entirely based on a slight tilting of CuO_6 octahedra.[11] However, as the temperature is decreased below 70 K, the temperature dependence of both $\nu_Q(A)$ and $\nu_Q(B)$ changes, and both *A* and *B* lines display an identical drop in intensity and both nearly disappear by 15 K.[11] This drop in signal intensity is ''wipeout.'' As previously noted by Singer *et al.*, the estimation of the NQR intensity close to the onset of wipeout is made more difficult due to the change in the form of the spin-echo decay. Given the uncertainties in fitting the spin-echo decay, it is impossible to define T_{NQR} with an accuracy exceeding $\pm 10\%$.[11] Within these uncertainties, the onset of wipeout, T_{NQR}, is indistinguishable from T_{charge} for $x\approx\frac{1}{8}$. The wipeout and subsequent recovery

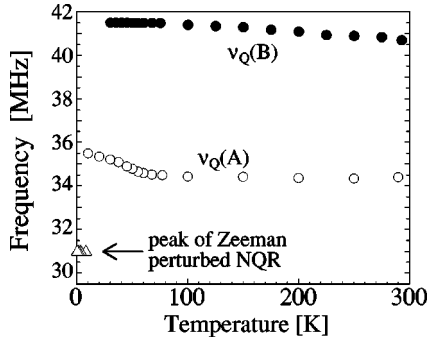

FIG. 4. The quadrupole resonance frequency $^{63}\nu_Q$ observed at fixed pulse separation time $\tau=12$ μsec for the *A* line (○) and *B* line (●) of a ^{63}Cu-isotope-enriched sample of $La_{1.875}Ba_{0.125}CuO_4$, as well as the peak frequency of the low-temperauture, Zeeman-perturbed NQR spectra (△).

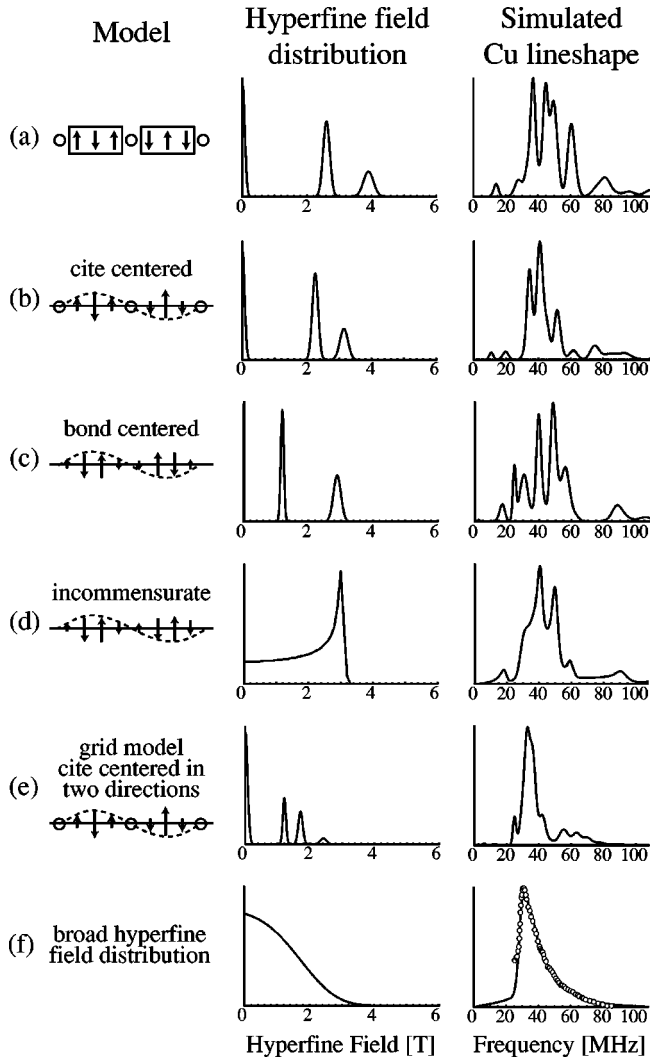

FIG. 5. Numerical simulations of the ^{63}Cu spectra based on several microscopic stripe models. The first column gives a schematic diagram of the orientation and magnitude of the Cu magnetic moments along the Cu-O bond direction. Arrows and open circles represent ordered Cu moments and a hole-rich antiphase boundary without an ordered moment, respectively. The middle column displays the expected distribution of the hyperfine magnetic field at the Cu sites. The right column contains the corresponding simulated line shape. (a)–(c) represent several commensurate stripe models, and an incommensurate spin density wave is presented in (d). Model (e) is a two-dimensional sinusoidal grid structure in the CuO_2 plane and (f) depicts a simple, broad distribution of the hyperfine field that provides a good fit to the 350-mK $La_{1.875}Ba_{0.125}CuO_4$ data, which is included as open circles.

of the intensity below 15 K will be analyzed in detail in Sec. IV. As the temperature is decreased below 8 K, the resonant signal begins to reemerge. This new line is shown in the bottom panel of Fig. 2. We note that the character of the line is entirely altered. The peak has shifted down in frequency from 35.5 MHz to 31 MHz. Additionally, the full width at half maximum (FWHM), which slowly increases with decreasing temperature from 2.0 MHz at 300 K to 2.6 MHz at 70 K to 3.2 MHz at 15 K, shows sudden and dramatic broadening to more than 12 MHz at 350 mK with the emergence of a large tail towards higher frequencies. Note that the spectra at 1.7 K and 350 mK are of identical shape and differ only in magnitude. In fact, the curves through those data sets in Fig. 2 are identical except for vertical scaling. Based on the analysis presented in the following two sections, we demonstrate that these changes are consistent with a broad distribution in the hyperfine magnetic field $\langle H_i \rangle$ averaged over NQR time scales.

C. Numerical simulations in standard stripe models

At the time of the discovery of stripes in Nd-doped $La_{1.48}Nd_{0.40}Sr_{0.12}CuO_4$ by neutron scattering,[2] Tranquada *et al.* proposed a simple model valid at the short time scale of neutron scattering (1 meV $\approx 2.4\times10^{11}$ Hz, corresponding to 4 psec) which consists of sets of three magnetic rows (a ''stripe'') separated by a charge-rich river which serves as an antiphase boundary for the antiferromagnetic order. This scenario is shown in Fig. 5(a). If the descriptions of the spin and charge density modulation based on this model and similar models as shown in Figs. 5(b)–5(e) (which are consistent with the neutron data) are valid for the entire sample at the much slower NQR time scale of ~ 20 μsec, we would expect inequivalent Cu sites. In the case of the model of Fig. 5(a), we expect there to be three inequivalent Cu positions: one site in the middle of the magnetic region, one at the edge, and one in the charge-rich river. As a first approximation, we expect the two magnetic sites at the center and edge of the stripe to yield three NMR lines each, while the nonmagnetic boundary site should produce a single NQR line. Thus, we might expect a total of at least seven resonance lines. These lines are not identifiable in the data.

Given that the 350 mK line shape shown in Fig. 2 is lacking the expected structure, we turn to numerical simulations by solving the Hamiltonian exactly. Using I as the nuclear spin, η as the asymmetry parameter of the electric field gradient (EFG), γ_n as the gyromagnetic ratio, h as Planck's constant, and $\mathbf{H}$ as the static hyperfine magnetic field, the Hamiltonian can be written as[41,42]

$$\mathcal{H}=\frac{\nu_Q h}{2}\left\{I_z^2-\frac{1}{3}I(I+1)+\frac{1}{6}\eta(I_+^2+I_-^2)\right\}-\gamma_n h\mathbf{H}\cdot\mathbf{I}, \tag{3}$$

where the ^{63}Cu nuclear spin is $I=\frac{3}{2}$ and the quadrupole resonance frequency $^{63}\nu_Q$, is related to the electron charge e, the maximum of the EFG q, and the ^{63}Cu quadrupole moment ^{63}Q, by

$$^{63}\nu_Q=\frac{3e^2q}{2hI(I+1)}{}^{63}Q. \tag{4}$$

Because of local axial symmetry of the Cu sites, the electric field gradient is nearly axially symmetric in both undoped and hole-doped CuO_2 planes. Additionally, as originally shown by Ohsugi *et al.*[39,40] the ^{139}La NQR line broadening takes place only for the $|\pm\frac{1}{2}\rangle\leftrightarrow|\pm\frac{3}{2}\rangle$ transition in the low-temperature striped phase (also see Sec. III G). This indicates that the internal field lies primarily in the CuO_2 plane for $x\approx\frac{1}{8}$.[62,63] Under these conditions, the Hamiltonian from Eq.

(3) is greatly simplified and can be written in matrix form, where we chose the basis to be the eigentates of the operator I_z:

$$\mathcal{H}=h\begin{bmatrix} \frac{-6\gamma_n H-\nu_Q}{4} & 0 & \frac{\sqrt{3}\nu_Q}{4} & 0 \\ 0 & \frac{-2\gamma_n H+\nu_Q}{4} & 0 & \frac{\sqrt{3}\nu_Q}{4} \\ \frac{\sqrt{3}\nu_Q}{4} & 0 & \frac{2\gamma_n H+\nu_Q}{4} & 0 \\ 0 & \frac{\sqrt{3}\nu_Q}{4} & 0 & \frac{6\gamma_n H-\nu_Q}{4} \end{bmatrix} \tag{5}$$

Between the four eigenstates of the Hamiltonian, there are six possible transitions corresponding to six resonant frequencies as shown in Fig. 1. Some of these transitions are nearly forbidden by the $|\Delta m|=1$ selection rule and exist only due to the unusual mixing of states that occurs in the low- and intermediate-field regions where $\gamma_n H \lesssim \nu_Q$. Thus we must consider the probability for each transition to occur. Following Muha,[64] we treat the small experimentally induced field $\mathbf{H}_1$ (~ 100 G) as a perturbation and use the the standard time-dependent expression for the transition rate between two states n and n':

$$P_{n,n'}=|\langle n'|\mathbf{I}\cdot\mathbf{H}_1|n\rangle|^2. \tag{6}$$

Since we are working on polycrystalline samples where the direction of $\mathbf{H}_1$ with respect to the crystal axis is random, we perform a powder average to obtain the probability for each transition. These probabilities correspond to the expected intensity for each resonance line in Fig. 1. Full line shape simulations are computed numerically by summing contributions from distributions in both the hyperfine field and in the quadrupole frequency. If the charge density modulation is sizable, $^{63}\nu_Q$ may vary depending on the site, and the axial symmetry of the EFG tensor can break down. However, the structureless broad resonance line observed below 8 K suggests that the spatial modulation of spin and charge is smooth at the NQR time scale $\tau_{NQR}\approx 10^{-5}$ sec. Hence we believe that approximating the quadrupole tensor as axially symmetric is acceptable in our simulations. Extrapolating from observations above 70 K before wipeout begins we find $^{63}\nu_Q(A)=34.5$ MHz for the A site and $^{63}\nu_Q(B)=41.8$ MHz for the B site. Note that, although the apparent peak frequency of the A line increases somewhat below 70 K as shown in Fig. 4, $^{63}\nu_Q(A)=35.5$ MHz at 10 K is achieved only for several percent of the sample. It is not initially clear what distribution of quadrupole frequencies to employ at low temperatures, where we expect charge order to induce an added width. In this section, we take both the A and B lines to be Gaussians, each with a width of 5.6 MHz (full width at half maximum), corresponding to twice the value extrapolated from the A line data above 70 K. We discuss the effects of differing amounts of quadrupole broadening in Sec. III E. To allow direct comparisons to the data, the simulated intensities are weighted by the square of the resonant frequency to account for experimental sensitivity.[41]

The next step is to estimate the distribution of the hyperfine magnetic field in various stripe models. First we examine the aforementioned model that was initially proposed by Tranquada *et al.*,[2] which is shown schematically on the left side of Fig. 5(a). The Cu site in the middle of the magnetic "stripe" is locally in the same environment as in the antiferromagnetic Néel state, so we expect the field at the nucleus to be $H^{center}=|A_x-4B|\mu_{eff}$ with an effective magnetic moment of $\mu_{eff}=0.3\mu_B$.[27,29,31] Inserting this value and the hyperfine coupling constants discussed above in Sec. III A, we estimate $H^{center}=130$ kOe/$\mu_B\times 0.3\mu_B=3.9$ T. For the Cu site at the edge of the stripe, there are only three magnetic nearest-neighbor sites that give rise to supertransferred hyperfine fields, so the expected field is $H^{edge}=|A_x-3B|\mu_{eff}=2.6$ T. The last Cu site is within the antiphase boundary, where we expect oppositely oriented magnetic contributions from two nearest neighbors which cancel, yielding $H^{boundary}=0$. We plot these values of H^{center}, H^{edge}, and $H^{boundary}$ in the distribution of the internal field at the top center of Fig. 5, where the vertical scale is determined by the relative numbers of each Cu site, which is the integral of each peak. The widths are chosen as depicted in the figure, where for $H>0$ the widths are proportional to the hyperfine field H as would be expected for magnetic broadening. The numerically computed ^{63}Cu line shape is shown at the right of Fig. 5(a). Agreement between the data and the simulated line shape is poor. Specifically, all of the structures are too sharp, and even the largest peak is located at ~ 37 MHz, above the 31-MHz peak seen in the data.

In addition to the original model proposed by Tranquada *et al.*, we examine site-centered and bond-centered commensurate sinusoidal spin density waves and an incommensurate sinusoidal spin density wave, as well as a grid model (site-centered sinusoidal spin density wave in two directions) as shown in Figs. 5(b)–5(e). In each case $\mu_{eff}=0.3\mu_B$ represents the magnitude of the maximum moment. For each model, we follow the same procedure as outlined above to construct a hyperfine distribution and compute an expected ^{63}Cu line shape. In each of the simulated line shapes there is too much structure for a good match to the smooth data.

Even though agreement between the experimental spectra and the numerically simulated line shapes is poor, we notice that, in Figs. 5(d) and 5(e), there is substantial simulated signal at an experimental peak frequency of 31 MHz. These contributions do not arise from the details of the hyperfine field distribution, but rather from the nature of the transition energy levels themselves. If we look back at Fig. 1, we note the two transitions that start at $\nu_Q=34.5$ MHz and move to lower frequencies with increasing field. These lines achieve a broad minimum at 31 MHz. Because of the high density of states that corresponds to resonant frequencies near 31 MHz, *any continuous distribution* of internal fields that includes contributions in the broad window from 0.5 T to 2.5 T will give rise to a line shape with a 31-MHz peak. With this in mind we examine broad distributions of the hyperfine field,

and by trial and error we achieve a good fit to experimental data as shown in Fig. 5(f). In Sec. III E we will return to the issue of the low-temperature line shape to understand the magnetic state of the Cu-O plane at the slow time scales of our pulsed NQR experiments.

D. Recovered ^{63}Cu NQR intensity at 350 mK

So far we have considered only the line shape. Another important point that needs to be addressed is the integrated NQR intensity at 350 mK. An accurate measurement of the recovered integrated NQR intensity below 8 K is not easy. The ^{63}Cu NQR line shape measurements above 10 K can be performed in one single scan over frequency without changing the experimental setup, but the Zeeman-perturbed NQR line shape is so broad that we need to replace the rf coil of the tuned LC circuit in our NMR probe 3 or 4 times to cover the entire frequency range from 20 to 90 MHz. This enhances the uncertainties in our estimate of the integrated intensity, and this is the primary reason why we have large error bars for the integrated intensity below 8 K in Fig. 3. In addition, the line shape below 25 MHz is superposed by an order-of-magnitude stronger ^{139}La NQR line centered at 18 MHz. This does not allow us to measure the ^{63}Cu Zeeman-perturbed NQR intensity below 25 MHz. Above 70 K, earlier high-field measurements for an aligned powder sample guarantee that there is no NQR line below 25 MHz.[33] Within the large uncertainties, the recovered signal intensity integrated above 25 MHz represents only 50^{+30}_{-20} % of the value above 70 K. However, it is important to notice that for hyperfine fields ranging up to $\sim$4 T, there are two branches of Zeeman-perturbed NQR transitions below 25 MHz in Fig. 1. Within our model the calculations of Fig. 5(f) which correctly reproduce the line shape, we can estimate the fraction of integrated NQR intensity expected to appear below 25 MHz, which is 39%. It should be emphasized that the echo intensity for the simulated line shape plotted in Fig. 5(f) is scaled by multiplying by the square of the frequency to take into account the experimental sensitivity. Accordingly, the apparent integrated intensity below 25 MHz incorrectly appears to be a tiny fraction of the whole line shape. In other words, the maximum integrated intensity expected to reemmerge above 25 MHz is 61% of that at 70 K, as shown by a horizontal arrow in Fig. 3. This means that the experimentally observed intensity at 350 mK is effectively 82^{+49}_{-33} % of that at 70 K, accounting for nearly the full intensity from the sample. This rules out the possibility that the descrepancy between the experimentally observed Zeeman-perturbed NQR line shape and theoretical calculations based on stripe models originates from a missing intensity.

E. Numerical simulations based on stripe models including broadening and motional narrowing

The good agreement between the data at 350 mK and the simulated line shape and its integrated intensity based on the broad distribution of Fig. 5(f) indicates that the hyperfine field averaged over NMR time scales and over the entire sample should extend up to about 3 T with substantial weight

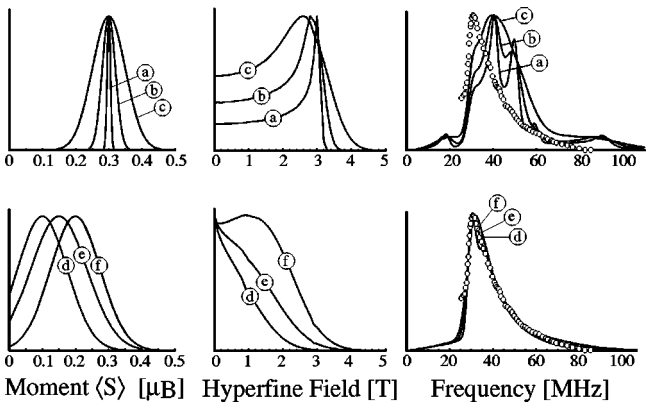

FIG. 6. Models of incommensurate spin density waves based on a distribution of the maximal moment in different segments of the sample as given in the leftmost column. Corresponding to these distributions we plot the hyperfine field at the nuclear site in the middle column and the simulated ^{63}Cu line shape at the right. In models (a)–(c) and (e) we assume a quadrupole width of 5.6 MHz; in (d) that width is taken to be 7.5 MHz and in (f) 3.7 MHz. The 350-mK spectra data are shown as open circles.

in the region below 2 T. Motivated by the success of the fit for the broad distribution of hyperfine fields, we return our attention to the stripe models of Figs. 5(a)–5(e) to examine the possibility that the internal hyperfine field corresponding to the stripe models may be broadened, either by disorder within the sample or by motional averaging effects, in such a manner as to be consistent with the ^{63}Cu NQR spectra.

In Fig. 6 we develop the hyperfine field distribution expected from an incommensurate spin density wave, favored by a recent μSR study,[31] including varying amounts of broadening, and calculate the corresponding simulated ^{63}Cu line shape. We take the magnitude of the maximum spin in different regions of the sample to be $\langle S\rangle$, which may be distributed due to static inhomogenieties. We numerically simulate the hyperfine field based on a row of 10 000 electron spins of magnitude $\langle S_n\rangle = \langle S\rangle \sin[2\pi n/(8+\delta)]$ with $|\delta| \ll 1, \delta \neq 0$, taken to be aligned along the x axis and labeled by position n. The spatial periodicity is that expected from neutron data.[2] The internal field at each site is computed with the use of Eq. (1), giving $\langle H_n\rangle = A_x\langle S_n\rangle - 2B\langle -S_n\rangle - B\langle S_{n+1}\rangle - B\langle S_{n-1}\rangle$, where we assume Néel order in the y direction and use the values of A_x and B as given above. Distributions arising from different segments of the sample (different $\langle S\rangle$ values) are combined as per the distribution in $\langle S\rangle$. In Figs. 6(a)–6(c) we show three simulations based on distributions in the magnetic moment that are centered at $0.3\mu_B$. With increasing width in $\langle S\rangle$, both the hyperfine distributions and the simulated line shapes become more smooth. However, the smoothed line shapes are shifted to too high a frequency to match the experimental data. Thus we rule out the possibility of a *static* incommensurate spin density wave *at NQR time scales* with maximum magnetic moment of $0.3\mu_B$, even with possible broadening of the value of the moment.

Next we consider the possibilities of a smaller average-ordered moment and of a different amount of quadrupolar broadening. The simulations of Figs. 6(d)–6(f) represent good fits to the data based on average-ordered moments of

$0.10\mu_B$, $0.15\mu_B$, and $0.20\mu_B$ paired with quadrupole widths of 7.5, 5.6, and 3.7 MHz, respectively. Without this extra quadrupole broadening the contributions of the *A* and *B* lines give rise to distinct peaks in the simulated line shape, in contradiction with our experimental findings. In the homogenously doped CuO_2 planes of $La_{2-x}Ba_xCuO_4$ with $x \gtrsim \frac{1}{8}$ the doping dependence of $\nu_Q(A)$ is known.[59] If we imagine the system to consist of many patches, each of which being homogenously doped, the extra width in $\nu_Q(A)$ beyond the extrapolated value from $T > T_{charge}$ (2.8 MHz) would correspond to distributions in x of approximate width $\Delta x \approx 0.30$, 0.18, and 0.06, respectively. There is a trade-off between the broadening caused by the magnetic effects and that caused by inherent distribution of the quadrupole resonance. However, the simulated line shape of Fig. 6(e) best fits the data, indicating that within that incommensurate spin density wave model a distribution of $\langle S \rangle$ centered at $0.15\mu_B$ coupled with moderate quadrupolar broadening corresponding to $\Delta x \approx 0.18$ provides the best fit to the data, although there is a range of parameters ($\langle S \rangle$ and quadrupole width) that provide a reasonable fit to the data, as indicated in Figs. 6(d) and 6(f). Of course, this model assumes patches of homogenious doping rather than microscopic structure (stripes) which represents an alternative, and perhaps more likely, path to increased width in ν_Q.

How can we reconcile this result with the conclusion of Kojima *et al.*[31] based on their μSR data? Kojima *et al.* observed a well-defined precession of positive muons consistent with an incommensurate spin density wave with a well-defined maximum ordered moment of $0.3\mu_B$.[31] If we recall that muon spin precession persists for only about 0.5 μsec, while the NQR spectrum is obtained by spin-echo measurements that detect a hyperfine field averaged over 20 μsec, one possible explanation is that the relatively large and well-defined moment of $0.3\mu_B$ observed by μSR measurements[27,29,31] is still slowly fluctuating during the duration of a Zeeman-perturbed NQR measurent. Since the hyperfine field is a vector quantity, the averaging process will always reduce the apparent, averaged field. Thus, the effect of motional averaging will be to pull all instantaneous values of the hyperfine field towards zero, reducing the effective values. This may be the key to resolving the apparant discrepancy between our NQR findings and the μSR measurements. We recall that resistivity never diverges in the stripe phase,[21,22] and hence we believe that mobile holes disrupt spin order. We note that the motional averaging scenario is supported by the large value of $^{139}1/T_1T$ at 350 mK (see Fig. 17), which indicates that low-frequency spin fluctuations persist even at our experimental base temperature. We also note that the motional averaging effects in the present case of Zeeman-perturbed NQR are somewhat different from the textbook cases[41,42] of *motional narrowing* and *exchange narrowing*. In those cases, one applies a strong and static external magnetic field to observe NMR signals. The applied field defines the Larmor precession frequency of nuclear spins, and the dipole line brodening is only a small perturbation. In the present case, however, the fluctuating hyperfine field caused by freezing Cu moments is comparable to or even greater than the unperturbed NQR frequency. Thus, as long as very slow fluctuations exist in the hyperfine field, the Larmor precession itself is not well defined. Accordingly we expect that our Zeeman-perturbed NQR spectra is extremely sensitive to very slow fluctuations of the hyperfine field. It is worth noting that our case resembles the motional narrowing considered by Kubo and Toyabe for zero or small field resonance[65] that has been applied to the analysis of μSR data in glassy systems.[66]

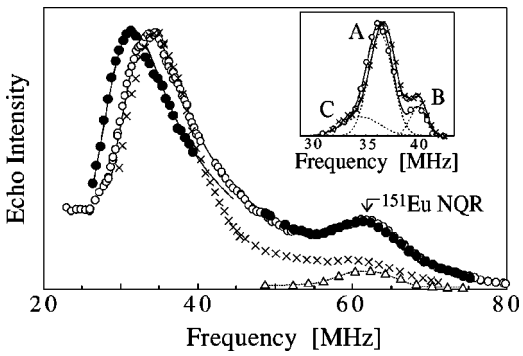

FIG. 7. Resonance spectra at 1.7 K with a pulse separation time of $\tau = 12$ μsec for single isotope-enriched samples of $La_{1.8-x}Eu_{0.20}Sr_xCuO_4$ [^{63}Cu, $x=0.12$ (○); ^{65}Cu, $x=0.12$ (●); ^{63}Cu, $x=0.16$ (×)]. Data taken with longer $\tau = 100$ μsec on the ^{65}Cu-enriched sample is marked by △. The solid curves represent numerical simulations of the $x=0.12$ data as described in the text, while the dotted curve is a guide for the eye. Inset: 100-K line shapes for the ^{63}Cu-enriched samples using the same symbols as above. In the inset the solid curves represent the sum of three Gaussians representing the *A*, *B*, and *C* peaks, which are individually depicted by dashed curves for the $x=0.12$ sample. For both cases the intensity ratio $A:B:C$ is consistent with the expected form $0.8-x:x:0.2$ from Cu sites away from all dopants, closest to the Sr ions and next to the Eu dopants, respectively.

Although we have focused on the incommensurate spin density wave model here, the possibilities of static broadening and motional averaging can be applied to all of the models presented in Fig. 5. In each case the sharp structures can be smoothed out by inhomogeneities within the sample or by motional effects, and the hyperfine field distributions can be made to be similar to that of Fig. 5(f) and, hence, with the experimental data. Thus, we cannot exclude any of the stripe models in Fig. 5 based on our simulations.

F. ^{63}Cu and ^{65}Cu resonance spectra in $La_{1.68}Eu_{0.20}Sr_{0.12}CuO_4$ and $La_{1.64}Eu_{0.20}Sr_{0.16}CuO_4$

In Fig. 7 we show the Zeeman-perturbed NQR spectum for two samples of $La_{1.68}Eu_{0.20}Sr_{0.12}CuO_4$, one enriched with the ^{63}Cu isotope and the other with ^{65}Cu. The peak frequency of the major peak is 34 ± 0.75 MHz for the ^{63}Cu-enriched sample and 31 ± 0.75 MHz for the sample enriched with ^{65}Cu. The peak frequency of the ^{63}Cu sample is 3 ± 1.5 MHz higher than the 31 MHz observed for ^{63}Cu in $La_{1.875}Ba_{0.125}CuO_4$. The shift of the Zeeman-perturbed NQR peak between these two materials arises primarily from the difference in the intrinsic quadrupole frequencies, which is 2.0 MHz at 70 K. Additionally, the greater proximity of the *B* line in the Eu-codoped material (see the inset of Fig. 7) con-

tributes to a higher peak frequency in the Zeeman-perturbed spectra, whereas the greater separation of the *B* line in $La_{1.875}Ba_{0.125}CuO_4$ results in an increased width.

The only extra feature visible in these line shapes for the Eu-doped materials as compared with those of $La_{1.875}Ba_{0.125}CuO_4$ (recall Fig. 2) is the peak at 62 MHz. We also observed extremely weak signals that continue above 80 MHz. We believe that these signals arise from NQR of the Eu nuclei themselves. We note that the peak at 62 MHz is observed only in the Eu-doped materials and is independent of the Cu isotope present in the ^{63,65}Cu-isotope-enriched samples. The relaxation time at the 62-MHz peak is also slow, allowing us to use an increased delay time τ to separate it as shown by open triangles in Fig. 7(a). The reduced relaxation rate is consistent with the small hyperfine field expected at the Eu site, which is substituted at the La position. Furthermore, if we assume that the electric field gradient is the same at the Eu and La positions, use the ratio of the quadrupole moments for the two nuclei ($^{151}Q/^{139}Q=4.5$), and employ Eq. (4), we find that the expected peak position of ^{151}Eu NQR is $^{151}\nu_Q=59.5$ MHz, very similar to our observation. Finally, we note that the ^{151}Eu peak is still observed at 77 K, strongly indicating that there is no connection with the low-temperature Cu spectra.

Disregarding the Eu NQR signal, we focus on the Cu resonance in $La_{1.68}Eu_{0.20}Sr_{0.12}CuO_4$ below 55 MHz. We repeat the same line shape analysis as discussed above in Sec. III C for the Eu-doped materials. We substitute $^{63}\nu_Q(A)=36.2$ MHz, $^{63}\nu_Q(B)=40.2$ MHz, and $^{63}\nu_Q(C)=34.5$ MHz as extrapolated from temperatures above the onset of wipeout and include the slightly greater ($\sim$25% greater than the 5.6 MHz used in Fig. 5) width in quadrupole frequencies that is characteristic of the Eu-doped materials. We employ the same distribution of hyperfine magnetic field as above for $La_{1.875}Ba_{0.125}CuO_4$ [see Fig. 5(e)]. For the ^{65}Cu-isotope-enriched sample we use the ratio of qudrupole moments ($^{65}Q/^{63}Q=0.924$) and the gyromagnetic ratios ($^{65}\gamma/^{63}\gamma_n=1.071$) between isotopes to determine $^{65}\nu_Q(A,B)$ and to scale the response to the hyperfine field. In this way, there are no free parameters in the fit of either the ^{63}Cu or the ^{65}Cu spectra. The numerically calculated line shapes are shown in Fig. 7(a) as solid lines. The good agreement between these simulated line shapes with the experimental data for both isotopes supports the Cu spectra analysis that has been presented throughout Sec. III.

In order to investigate the influence of different hole concentrations on Zeeman perturbed ^{63}Cu NQR spectra, we carried out preliminary measurements in ^{63}Cu-isotope enriched $La_{1.64}Eu_{0.20}Sr_{0.16}CuO_4$. The recovered integrated intensity at 1.7 K is more than a factor of 2 smaller than in $La_{1.68}Eu_{0.20}Sr_{0.12}CuO_4$ [see Fig. 10(c)], in agreement with Teitel'baum *et al.*[13] The overall line shape presented in Fig. 7 is very similar to the case of $La_{1.68}Eu_{0.20}Sr_{0.12}CuO_4$, but the high-frequency tail is smaller and the width of the main peak 10.5 ± 0.5 MHz is narrower than 12.5 ± 0.5 MHz in $La_{1.68}Eu_{0.20}Sr_{0.12}CuO_4$. Within the line shape analysis presented above in Sec. III, this change in width implies that the maximum magnitude of the hyperfine field in $La_{1.64}Eu_{0.20}Sr_{0.16}CuO_4$ is 5–10% smaller than in $La_{1.68}Eu_{0.20}Sr_{0.12}CuO_4$ at 1.7 K. There are a few possible explanations for the difference in hyperfine field. First, since stripes are less stable at hole concentrations $x\neq\frac{1}{8}$,[11,13,28,39] there may be additional fluctuations for those concentrations that may motionally narrow the main peak. This picture is consistent with the fact that at 1.7 K, a smaller fraction of the Cu signal intensity reemerges as Zeeman-perturbed NQR in the samples away from $x\approx\frac{1}{8}$.[13] Second, it is possible that the increased disorder caused by the additional holes may increasingly frustrate the spins and reduce the magnitude of ordered moments. We also note that the peak is slightly higher in the $x=0.16$ material as compared to $x=0.12$, because $\nu_Q(A)$ increases with hole doping.

Before closing this section we would like to comment breifly on two recent reports of low-temperature ^{63}Cu NQR spectra in $La_{1.8-x}Eu_{0.20}Sr_xCuO_4$ (Ref. 13) and $La_{1.875}Ba_{0.125}CuO_4$.[67] Both of these publications show broad line shapes superposed with what appears to be a NQR signal from the high-temperature *A* and *B* lines that have survived to low temperature. We have seen comparable results on a poorly annealed sample of $La_{1.875}Ba_{0.125}CuO_4$ in which wipeout was not complete. After a careful reannealing of this sample, wipeout became complete and the *A* and *B* lines disappeared from the low-temperature spectra. We note that potential problems with the line shapes does not diminish the primary finding of Teitel'baum *et al.* regarding the doping dependence of the recovered signal, i.e., that the intensity of the recovered signal at 1.3 K in $La_{1.8-x}Eu_{0.20}Sr_xCuO_4$ is greatest for $x\approx\frac{1}{8}$, indicating the increased stability of that doping level.[13] This conclusion is in agreement with our earlier finding that the temperature dependence of wipeout effects in $La_{1.6-x}Nd_{0.40}Sr_xCuO_4$ is sharpest for $x\approx\frac{1}{8}$.[11] It is also consistent with another earlier finding based on hyperfine broadening of the ^{139}La NQR line at 1.3 K by Ohsugi *et al.* indicating that stripes are most stable near $x\approx0.115$ in $La_{2-x}Sr_xCuO_4$.[39]

G. ^{139}La NQR line shapes in $La_{1.875}Ba_{0.125}CuO_4$

To this point we have discussed only the results of ^{63,65}Cu NQR, but resonance studies of the ^{139}La site can also provide additional insight.[39,40,62] Since the ^{139}La nucleus has spin $I=\frac{7}{2}$, the ^{139}La NQR spectra of a single site consist of three peaks, roughly corresponding to 1, 2, and 3 times $^{139}\nu_Q$. With the addition of a perturbing magnetic field, the three resonance lines are split in a manner that depends on the details of the direction and the magnitude of the hyperfine field.[62] In earlier ^{139}La NQR studies of the low-temperature striped phase of $La_{2-x}Sr_xCuO_4$, Ohsugi *et al.* found that the $|\pm\frac{1}{2}\rangle\leftrightarrow|\pm\frac{3}{2}\rangle$ transitions at ~6 MHz broaden for $x\approx\frac{1}{8}$ at 1.3 K, while the $|\pm\frac{5}{2}\rangle\leftrightarrow|\pm\frac{7}{2}\rangle$ transitions at ~18 MHz do not show magnetic line broadening.[39,40] This implies that the time-averaged hyperfine field lies within the CuO_2 plane.[62,63] In this case, the extra line broadening is roughly equal to $4\gamma_n H_{ab}$, where H_{ab} is the hyperfine field.

Our goal is to use the broadening that we observe in the $|\pm\frac{1}{2}\rangle\leftrightarrow|\pm\frac{3}{2}\rangle$ ^{139}La NQR transition as a test of the models presented above in Sec. III C. We present the temperature dependence of the linewidth of the $|\pm\frac{1}{2}\rangle\leftrightarrow|\pm\frac{3}{2}\rangle$ ^{139}La

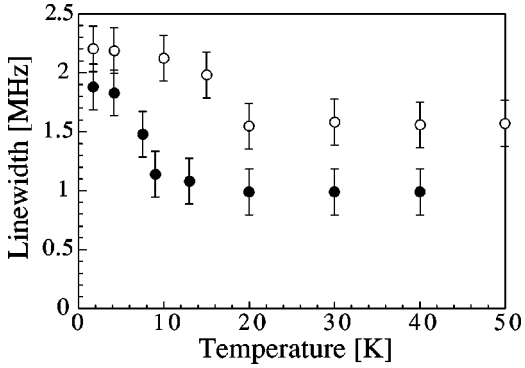

FIG. 8. ^{139}La linewidth as a function of temperature for the $|\pm\frac{1}{2}\rangle\leftrightarrow|\pm\frac{3}{2}\rangle$ transition at a frequency $^{139}\nu_Q\approx 6$ MHz for $La_{1.875}Ba_{0.125}CuO_4$ (●) and $La_{1.68}Eu_{0.20}Sr_{0.12}CuO_4$ (○).

NQR transition in Fig. 8 for $La_{1.875}Ba_{0.125}CuO_4$. Line shape data from the same sample are presented in Fig. 9. The linewidth broadens from 1.0 MHz at 20 K to 1.9 MHz at 1.7 K, but does not display the clear splitting that is observed in the Néel state of La_2CuO_4.[52,62,63] A similar temperature dependence was found in $La_{1.68}Eu_{0.20}Sr_{0.12}CuO_4$ as shown in Fig. 8. The increase of the linewidth at a somewhat higher temperature implies that the slowing of spin fluctuations is more rapid in $La_{1.68}Eu_{0.20}Sr_{0.12}CuO_4$ than in $La_{1.875}Ba_{0.125}CuO_4$, consistent with the larger $^{139}1/T_1T$ at the same temperature in the former material, as seen in Fig. 17(b). In a recent work, Teitel'baum *et al.* also found similar behavior for a Nd-doped sample with $x=0.12$.[68]

To test the consistency of the ^{139}La line broadening with the models proposed above to account for the ^{63}Cu Zeeman-perturbed line shape, we undertake an analysis very similar to that of Sec. III C. Again we perform an exact diagonalization of the Hamiltonian [Eq. (3)], but this time for spin $I=\frac{7}{2}$, employing the same value of η and the same small tilting of spin orientation as deduced by Nishihara *et al.*[62] We confirmed that our conclusions do not depend on small variations in these additional parameters. In the right-hand column of Fig. 9, we present three model hyperfine field distributions including (a) and (b) which are the same hyperfine field distributions as used in the ^{63}Cu line shape analysis as shown in Figs. 5(a) and 5(f). To avoid confusion, the magnitude of the hyperfine field is still specified by its value at the ^{63}Cu site, although its value is greatly decreased at the ^{139}La position because of the two orders of magnitude smaller hyperfine coupling constant. Specifically, we take the ratio of the hyperfine field at the ^{139}La and ^{63}Cu sites to be the same as in undoped La_2CuO_4, which is 0.1 T/8.2 T=0.012. [63,50] This means that if there is 4 T of hyperfine field at a Cu site, there is 0.048 T of hyperfine field at nearby La sites. We must caution that this ratio can, in principle, be dependent on the exact material chosen and especially on low-temperature structural transitions which alter the mixing of atomic orbitals. In addition, if there is a strong modulation of the hyperfine field at nearby Cu sites, the La ions may experience an average of those values. However, we find that the use of this ratio 0.012 adequately describes our data. Finally, we take the 20 K ^{139}La NQR data of Fig. 9 and numerically simulate the added width that arises from the static hyperfine field distributions given by the distributions (a)–(c) of Fig. 9. These simulated low-temperature line shapes are depicted as solid lines in the main panel of Fig 9. We note that the differences between the simulated line shapes corresponding to the different hyperfine field distributions are small, indicating that it is impossible to choose one over another based on the ^{139}La NQR measurement alone. However, we also note that all are consistent with the observed broadening of the ^{139}La NQR line shape, giving added weight to the correctness of our explanation of the ^{63,65}Cu and ^{139}La spectra in $La_{1.875}Ba_{0.125}CuO_4$ as presented throughout this section.

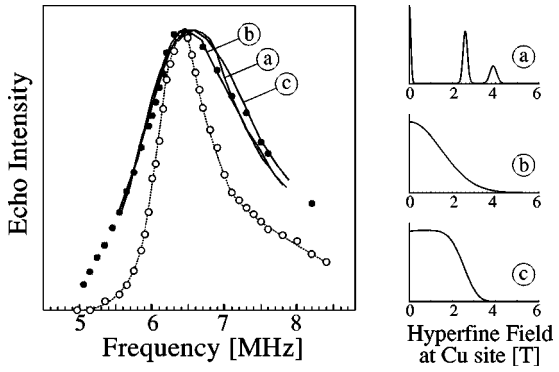

FIG. 9. ^{139}La NQR spectra of $La_{1.875}Ba_{0.125}CuO_4$ for the $|\pm\frac{1}{2}\rangle\leftrightarrow|\pm\frac{3}{2}\rangle$ transition at 20 K (○) and 1.7 K (●) in the main plot to the left. The solid lines represent simulated line shapes that arise from three different distributions of internal hyperfine magnetic field as discussed in the text. The hyperfine distributions are depicted in the small plots to the right and are labeled (a)–(c) to match the corresponding simulated line shape.

H. Summary of Zeeman-perturbed NQR line shape measurements and analysis

We have demonstrated that for $La_{1.875}Ba_{0.125}CuO_4$, $La_{1.68}Eu_{0.20}Sr_{0.12}CuO_4$, and $La_{1.64}Eu_{0.20}Sr_{0.16}CuO_4$, the ^{63}Cu NQR signal that is wiped out at high temepratures reemerges below ~8 K as a single, broad peak with a lower peak frequency. The broad linewidth is caused by hyperfine magnetic fields from frozen Cu magnetic moments that are nearly static over NQR time scales. The hyperfine field H is primarily within the CuO_2 planes and the hyperfine fields extend up to 3–4 T. The upper bound of the field distribution corresponds to the maximum frozen Cu magnetic moments of $0.2\mu_B$–$0.3\mu_B$, in rough agreement with estimates based on μSR. However, the field distribution is not consistent with the sharply defined stripe models that properly account for the elastic neutron scattering data and the precession of muons at faster time scales.

To fit the Zeeman-perturbed NQR within the stripe models, including the incommensurate spin density wave picture that is favored by μSR, the observed line shape requires a field distribution centered close to zero with a very large distribution coupled with an increased quadrupole width. The magnitude of the corresponding maximum Cu magnetic moments, $\sim 0.15\mu_B$, is suppressed relative to the $\sim 0.3\mu_B$ as

determined by μSR studies. This, together with somewhat narrower line shape observed for $La_{1.64}Eu_{0.20}Sr_{0.16}CuO_4$ and the relatively high relaxation rate $^{139}1/T_1T$ observed even at 350 mK, indicates that motional narrowing is caused by remnant slow fluctuations which persist even at our base temperature. The presence of slow fluctuations has also been emphasized by Suh *et al.*[69] The fact that the 1.7 K and 350 mK spectra are of identical shape suggests that the decreasing frequency scale of charge and spin fluctuations has saturated and that there are many low-lying excited states of the stripes, while the continuing NQR signal recovery may indicate that an increasing fraction of the sample is experiencing the saturated, low-frequency fluctuations.

The increased quadrupole width that is required to smooth the *A* and *B* lines into the low-temperature line shape indicate the presence of a broadly distributed charge environment which alters the electric field gradient site by site. Although we find in Sec. IV that we can phenomenologically account for the ^{63}Cu wipeout data based on slowing spin fluctuations, this quadrupole broadening indicates that spatial variation of the local charge environment does indeed exist throughout the sample.

IV. SLOWING OF THE FLUCTUATION TIME SCALE FOR THE $\frac{1}{8}$ PHASES

A. Preliminary considerations on the fluctuation frequency scales of stripes

In general, the growth of short-range antiferromagnetic spin-spin correlations causes the spin fluctuation frequency scale $\Gamma = 1/\tau_{spin}$ to gradually slow down. In the normal metallic state above T_c in the high-T_c cuprates, the characteristic fluctuation frequency Γ of spin fluctuations decreases roughly in proportion to the temperature *T*. This peculiar slowing down is frequently referred to as ''ω/T scaling,'' because the frequency dependence of $\chi''(\mathbf{q},\omega)$ satisfies a simple scaling law when the frequency ω is normalized by the temperature *T* (or, equivalently, by Γ).[43,44] One can define Γ as the peak frequency of the ω dependence of $\chi''(\mathbf{q},\omega)$ or, more precisely, by fitting $\chi''(\mathbf{q},\omega)$ to a relaxational function with appropriate frequency dependence. We fit $\chi''(\mathbf{q},\omega)$ observed by Aeppli *et al.*[45] for $La_{1.86}Sr_{0.14}CuO_4$ to a Lorentz oscillator form to deduce $h\Gamma \approx 8.8$ meV at 35 K. By scaling the magnitude of $h\Gamma$ obtained at 35 K for $La_{1.86}Sr_{0.14}CuO_4$ linearly with temperature, we estimate $h\Gamma \approx 17.6$ meV at $T_{charge} = 70$ K. Needless to say, $h\Gamma$ should depend on the hole concentration *x* [for example, $h\Gamma \approx 4$ meV at similar temperatures for $x = 0.04$ (Ref. 43)]. We expect a somewhat smaller value of $h\Gamma$ for $x = 0.12$ than for $x = 0.14$ because the dynamic spin-spin correlation length is somewhat longer for $x = 0.12$ than for $x = 0.15$.[70] However, since $^{63}1/T_1$ depends little on *x* for $0.12 \leqslant x \leqslant 0.20$, we do not expect a major change in the magnitude of $h\Gamma$. We note that $^{63}1/T_1$ in $La_{1.8-x}Eu_{0.2}Sr_xCuO_4$ is nearly identical with that of $La_{2-x}Sr_xCuO_4$. Hence, it is safe to assume that the spin dynamics above T_{charge} depends little on Eu or Nd rare-earth codoping.

The important point to notice is that this mild *T*-linear slowing down of spin fluctuations with temperature breaks down in the charge-ordered segments of the CuO_2 planes below $T_{charge} \approx 70$ K. EPR measurements by Kataev and co-workers[16] indicate that spin fluctuations are slowing more quickly below T_{charge}. Somewhat below the onset of charge ordering, spin fluctuations in some segments of the $La_{1.48}Nd_{0.4}Sr_{0.12}CuO_4$ sample become slow enough at $T_{spin}^{neutron} = 50$ K to be considered static, and neutron scattering measurements begin to detect quasielastic scattering with excitation energy $\hbar\omega \approx 1$ meV. We emphasize that this does not mean that all the Cu spins have slowed down to $\hbar\Gamma \approx 1$ meV. The fact that some Cu NQR signal is still observable even below T_{charge} and the $^{63}1/T_1$ measured for the observable segments does not show any anomalous behavior[10,11,33,56] indicates that the observable Cu NQR signals originate from other segments of the CuO_2 plane where Γ is still smoothly slowing following the ω/T scaling. One may imagine that phase separation sets in with microscopic length scales below T_{charge}, and Γ begins to exhibit a glassy slowing with a broad distribution because Γ slows down exponentially in the charge-ordered segments. This is in sharp contrast with the narrow and well-defined spin fluctuation frequency Γ in the ordinary metallic state of CuO_2 planes above T_{charge}. We also note that if charge order is a second-order phase transition, the critical slowing of charge dynamics should exist even above T_{charge}. In fact, the resistivity data do show an upturn prior to T_{charge}.[21,22] This means that precursors of glassy slowing may exist at temperatures slightly above T_{charge}. Our earlier observation that the Gaussian component of $^{63}1/T_2$ shows a gradual crossover to a Lorentzian component due to motional narrowing $\sim$10–30 K above T_{charge} supports this idea.

The inelastic magnetic neutron scattering intensity reaches about 80% of the maximum value by 25 K, meaning that 80% of the spins are slowed to below the time scale of $\tau_{neutron} \approx 10^{-11}$ sec by 25 K. To our knowledge, no detailed inelastic neutron scattering data are available for $La_{2-x-y}(Nd,Eu)_ySr_xCuO_4$ with $x \approx \frac{1}{8}$ near T_{charge} and T_{spin} other than a limited data set reported by Tranquada *et al.*[9] Accordingly, the details of how the slowing of spin fluctuations deviates from the high-temperature ''ω/T scaling'' towards $\hbar\Gamma \approx 1$ meV at 50 K as a function of temperature is unknown. In what follows we smoothly extrapolate the low-temperature behavior to the ω/T curve.

In this temperature range, μSR measurements do not detect any static hyperfine fields. This means that Cu spins fluctuate so quickly that the hyperfine field is averaged to zero. With decreasing temperature, μSR measurements begin to detect a static hyperfine magnetic field that last longer than 0.1 μsec between 25 and 30 K. This means that the spin fluctuation frequency Γ has slowed down to $\sim 10^7$ Hz in some segments of the CuO_2 planes. At 30 K, the Cu NQR signal is almost completely wiped out as shown in Fig. 3. This indicates that normal metallic segments of CuO_2 planes no longer exist below 30 K. By extending the ω/T scaling down to 30 K, we estimate the upper limit of the distribution of the spin fluctuation frequency $\Gamma \sim 10^{12}$ Hz at 30 K. On the other hand, the lower limit from the slowest components of spins is $\sim 10^7$ Hz.

The line broadening of Zeeman-perturbed NQR caused by static hyperfine magnetic fields takes place for ^{139}La NQR and ^{63,65}Cu at an even lower temperature, $T_{NQR}^{Zeeman} \approx 18$ K and 8 K, respectively (see Figs. 3 and 8). This indicates that the fluctuation frequency spectrum has slowed to a time scale comparable to the duration of a spin-echo experiment. This time scale is set by the separation of two rf pulses, usually $\tau = 12$ μsec; i.e., if spins fluctuate much slower than $h\Gamma \approx 10^5$ Hz, the hyperfine field would look entirely static and we expect full hyperfine broadening. As explained in Sec. III, our Zeeman-perturbed NQR results seem to indicate that this condition is not quite satisfied in the present case even at 350 mK. In Fig. 10 we present a summary of experimental information regarding the distribution of slowing spin fluctuations.

In the following sections, we will demonstrate that the glassy slowing of spin fluctuations below T_{charge} for $x \approx \frac{1}{8}$ can be explained consistently based on the renormalized classical scaling of the nonlinear σ model with a reduced value of spin stiffness $2\pi\rho_s^{eff}$. In Sec. IV B, we estimate the numerical value $2\pi\rho_s^{eff} \approx 200$ K based on a simple physical argument. We will also explain why the *indirect* spin contribution to wipeout can be triggerred by charge ordering. In Sec. IV C, we analyze the sudden and dramatic increase of $^{139}1/T_1T$ and its distribution that takes place below T_{charge} based on the renormalized classical scaling, and deduce the spatial distribution of Γ as a function of temperature. In Sec. IV D, we analyze ^{63}Cu and ^{139}La NQR wipeout effects together with magnetic neutron scattering and μSR data, again based on the renormalized classical scaling. The distribution of Γ deduced by this approach agrees well with that deduced from $^{139}1/T_1$.

B. Spin stiffness in charge-ordered segments and its relation to ^{63}Cu NQR wipeout

The ^{63}Cu nuclear spin-lattice relaxation rate $^{63}1/T_1$ diverges exponentially in the renormalized classical scaling regime of both isotropic[56] and anisotropic[72] quasi-two-dimensional (quasi-2D) Heisenberg systems. As shown in Fig. 11, an exponential divergence of $^{63}1/T_1$ was successfully observed in undoped La_2CuO_4, and the fit to the renormalized classical expressions allowed Imai *et al.* to estimate $2\pi\rho_s \approx 1730$ K.[56,73] Since $2\pi\rho_s = 1.13J$, this implies $J \approx 1500$ K, in good agreement with an estimation based on neutron and Raman scattering measurements.[74,75]

Naturally, one would expect that measurements of $^{63}1/T_1$ may allow us to determine the spin stiffness also in the striped phase below T_{charge}.[9,76] Unfortunately, $^{63}1/T_1$ measured for the *observable* ^{63}Cu NQR signal represents the spin fluctuation properties of the not-yet stripe-ordered segments (i.e., ω/T scaling), and exhibits little signature of exponential divergence even below 50 K,[11,77] where spin freezing is observed by neutron scattering. The absence of divergence in the measured value of $^{63}1/T_1$ can be understood based on the following considerations. First, we recall that, quite generally, nuclear relaxation rates are inversely proportional to the energy scales of spin fluctuations, such as

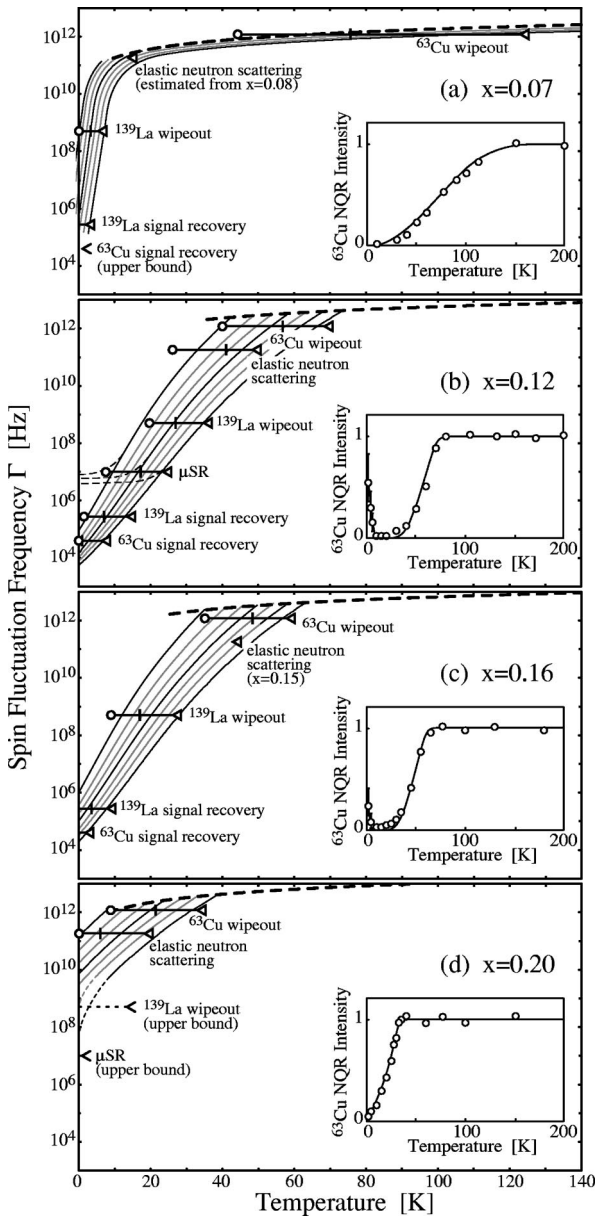

FIG. 10. The distributions of the spin fluctuation frequency Γ as a function of temperature for Nd- and Eu-codoped $La_{2-x}Sr_xCuO_4$ for several values of x. For each measurement, the triangles, the small vertical line segments, and the open circles correspond to the onset, the 50% point, and the 80% point of the anomaly, respectively. In some cases data are not available and we estimate values from similar samples, as noted in the figure. The vertical positioning of the points indicates the appropriate time scale for each measurement, as discussed in Sec. IV D. The thick dashed line across the top of each panel represents ω/T scaling where there is little distribution of Γ. The experimental data serve as anchoring points for the distribution of Γ that is used in the wipeout calculations, which is depicted as a contour plot utilizing the solid black and gray curves (Ref. 71). The region between any two adjacent curves represents 12.5% of the volume of the sample, with an additional 12.5% above the top curve and below the lowest. Dashed lines near $\Gamma \approx 6 \times 10^6$ Hz for $x = 0.12$ represent the distribution Γ deduced in the Gaussian model as discussed in the text. The insets show the ^{63}Cu wipeout data and the simulated wipeout based on Eq. (15).

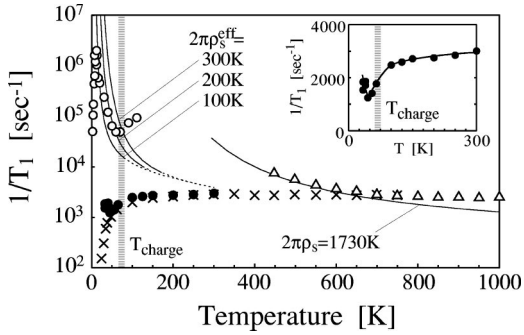

FIG. 11. $^{63}1/T_1$ data as a function of temperature for undoped La_2CuO_4 (Ref. 56) (△), $La_{1.85}Sr_{0.15}CuO_4$ (Ref. 56) (×), and $La_{1.68}Eu_{0.20}Sr_{0.12}CuO_4$ (Ref. 11) (●). We also show $^{139}1/T_1$ scaled by Eq. (7) for the Eu-codoped material (○). This quantity roughly represents $^{63}1/T_1$ of the unobservable ^{63}Cu NQR signal in the stripe-ordered segments. The curves represent $^{63}1/T_1$ in the renormalized classical scaling model with different values of $2\pi\rho_s^{eff}$ as listed. Inset: the same data for the Eu-codoped material on a linear scale for clarity.

$2\pi\rho_s$ and J.[78] Since $^{63}1/T_1$ in hole-doped high-T_c cuprates, including the striped phase, exhibits nearly identical values with undoped La_2CuO_4 at higher temperatures,[56] the fundamental energy scale of $^{63}1/T_1$ is set by the same bare J at high temperatures, even in the striped phase. On the other hand, from the measurements of the spin-spin correlation length, Tranquada *et al.* showed that the effective spin stiffness $2\pi\rho_s^{eff}$ is as small as ~ 200 K below T_{charge}.[9] We note that the fairly small spin stiffness can be considered a natural consequence of slowed charge dynamics, because a hole intervening the Cu-Cu exchange path would locally diminish the value of the exchange interaction J, and the effective spin stiffness $2\pi\rho_s^{eff}$ is essentially a spatial average of J at longer length scales.

We now recall that all of the ^{63}Cu NQR signal in high-T_c cuprates is near the detection limit of pulsed NQR experiments, and only a factor of ~ 3 enhancement in $^{63}1/T_1$ and an accompanying change in $^{63}1/T_2$ are sufficient to make signal detection impossible.[56,73] That is why ^{63}Cu NQR measurements in La_2CuO_4 could not be conducted below ~ 400 K.[56] The drastically reduced values of the spin stiffness in the charge-ordered segments mean that once the charge order sets in, $^{63}1/T_1$ and $^{63}1/T_2$ in those segments begin to blow up inversely proportional to $2\pi\rho_s^{eff}$. The fact that we do not observe a divergence of $^{63}1/T_1$ *for the observable parts of the NQR signal* near T_{charge} indicates that this divergence of $^{63}1/T_1$ in the charge-ordered segments takes place very quickly. In fact, as summarized in Fig. 10, the Cu spin fluctuation frequency decreases by $\sim 5-7$ orders of magnitude between 70 K and 350 mK, roughly an order of magnitude every 10 K. This provides a natural explanation of why the nuclear resonance signal from those segments experience dramatic and sudden wipeout due to the extremely fast relaxation times. This is the indirect spin contribution to wipeout triggered by charge order.[10,11]

Even though the wipeout of ^{63}Cu NQR prevents us from observing the renormalized classical behavior in the striped phase, one can utilize ^{139}La to probe the slowing of spin fluctuations. The hyperfine coupling between the Cu electron spins and ^{139}La nuclear spins is two orders of magnitude smaller than for the ^{63}Cu site. Since $1/T_1$ is proportional to the square of the hyperfine coupling, this means that, if we ignore nonmagnetic contributions to the relaxation, $^{139}1/T_1$ at the La sites is four orders of magnitude less sensitive to the divergence caused by the slowing Cu spin dynamics as compared with $^{63}1/T_1$ at the Cu site:

$$\frac{1}{^{139}T_1} \approx \left(\frac{^{139}\gamma_n}{^{63}\gamma_n} \frac{^{139}H_{hf}}{^{63}H_{hf}} \right)^2 \frac{1}{^{63}T_1} \approx (0.4\times 10^{-4}) \frac{1}{^{63}T_1}. \quad (7)$$

Thus the ^{139}La NQR signal does not suffer signal wipeout until the low-frequency spin fluctuations have slowed four more orders beyond the onset of ^{63}Cu wipeout. Accordingly, ^{139}La NQR $^{139}1/T_1$ is a better measure of spin fluctuations in the stripe-ordered segments of the CuO_2 planes below T_{charge}. However, we caution that $^{139}1/T_1$ is known to be dominated by processes other than Cu spin fluctuations above $T \sim T_{charge}$, most likely electric quadrupole coupling with lattice vibrations, making an interpretation of $^{139}1/T_1$ above T_{charge} difficult.

In Fig. 11 we plot both $^{63}1/T_1$ and $^{139}1/T_1$ for $La_{1.68}Eu_{0.2}Sr_{0.12}CuO_4$. As initially discovered by Cho and co-workers,[36,37] $^{139}1/T_1$ shows roughly exponential divergence below T_{NQR} in the underdoped regime of $La_{2-x}Sr_xCuO_4$. At $x=0$ the ^{63}Cu data fit well to the renormalized classical form in the low-T limit ($T \lesssim 2\pi\rho_s/2$), written as[79]

$$\frac{1}{T_1} = \frac{0.35}{Z_c} \frac{A_{\mathbf{Q}}^2}{J\hbar} \frac{\xi}{a} \frac{(T/2\pi\rho_s)^{3/2}}{(1+T/2\pi\rho_s)^2}, \quad (8)$$

$$\xi = 0.27 \frac{\hbar c}{2\pi\rho_s} \frac{\exp(2\pi\rho_s/T)}{1+T/2\pi\rho_s}, \quad (9)$$

with the $\mathbf{Q}=(\pi,\pi)$ component of the hyperfine coupling constant $A_{\mathbf{Q}}=A_x-4B$, the constant $Z_c=1.18$, and $2\pi\rho_s = 1730$ K. The spin-wave velocity is $c=\sqrt{2}JaZ_c/\hbar$. We also found similar behavior of $^{139}1/T_1$ in the striped phase of $La_{1.8-x}Eu_{0.2}Sr_xCuO_4$ and $La_{2-x}Ba_xCuO_4$ below T_{charge}, where the value of $2\pi\rho_s^{eff}$ is greatly reduced. In fact, from Fig. 11 we can estimate $2\pi\rho_s^{eff} \approx 200$ K, which is in good agreement with the previously mentioned result of neutron scattering, $2\pi\rho_s^{eff} = 200 \pm 50$ K.[9] It is important to notice that the extrapolation of the low-temperature renormalized classical fit to higher temperatures, as shown by the dashed curves in Fig. 11, overestimates $1/T_1$ observed for ^{63}Cu NQR by an order of magnitude above T_{charge}.

C. Spin fluctuation spectrum deduced from an analysis of T_1 recovery data

The renormalized classical (RC) expression for the nuclear spin-lattice relaxation rate $1/T_1$ [Eq. (8)] can be rewritten in terms of a frequency scale $\Gamma = (c/\xi)\sqrt{T/2\pi\rho_s}$ as

$$\frac{1}{T_1} = 0.49 \frac{A_{\mathbf{Q}}^2}{\hbar^2} \frac{1}{\Gamma} \frac{(T/2\pi\rho_s)^2}{(1+T/2\pi\rho_s)^2}, \tag{10}$$

which connects Γ to the observable quantity T_1, thus providing a natural route to obtain information on the fluctuation spectrum. Due to the strong wipeout of the ^{63}Cu NQR signal, we are forced to rely on the ^{139}La relaxation data, where wipeout is less severe and limited to the range 5–35 K (see Fig. 13 for wipeout data). We measure $^{139}1/T_1$ by the inversion-recovery method. The recovery of the nuclear magnetization may be fit to a solution to the standard rate equations,

$$\frac{m(t)}{m(\infty)} = 1 - \frac{3}{7} e^{-3t/T_1} - \frac{100}{77} e^{-10t/T_1} - \frac{3}{11} e^{-21t/T_1} \tag{11}$$

for the $|\pm\frac{5}{2}\rangle \leftrightarrow |\pm\frac{7}{2}\rangle$ NQR transition where $m(t)$ is the magnetization at a time t and $1/T_1$ is the single relaxation rate. This form is valid for magnetic relaxation when the spectral function is constant across the three NQR transitions, which is generally the case for $\Gamma \gg f_{NQR}$. At 65 K, the fit of the recovery data with a single value of T_1 is reasonably good, as seen in Fig. 12(a), but at 350 mK, the fit is quite poor. This led us to simulate the recovery curves due to distributions of T_1. The distributions in $1/T_1$ are displayed in the inset of Fig. 12(a), and the recovery is calculated by summing contributions from each segment of the sample, where the magnetization of each individual segment recovers per Eq. (11). These simulated recovery curves are plotted as solid lines in Fig. 12(a) and provide a much better fit to the 350-mK data, while slightly improving the quality of the fit at 65-K. The small distribution evident within the 65-K recovery data does not necessarily reflect an intrinsic distribution of the magnetic relaxation time T_1 but may be due to extrinsic processes such as quadrupole relaxation. In general, the central value of the T_1 distribution is very close to that which we find by force fitting to a single relaxation rate. As seen in Fig. 12(b), we found that the width w of the T_1 distribution increases with decreasing temperature below T_{charge} from $w \sim 20$ to $w \sim 200$–1000 at 1.7 K and below. The local minimum near 15 K is caused by the fact that ^{139}La NQR signals with extremely fast $^{139}1/T_1$ are effectively wiped out due to short T_2 relaxation rates (see Fig. 16); hence the measured nuclear spin recovery does not include those contributions. In the absence of those contributions, the width $w \sim 100$ near 15 K should be considered as a lower bound on w.

Using the RC form [Eq. (10)] with $2\pi\rho_s^{eff} = 200$ K we can convert these distributions of $1/T_1$ to Γ without any additional parameters. For $\Gamma \gg f_{NQR}$ the conversion is straightforward; these points are shown in Fig. 12(c). For Γ close to f_{NQR} the renormalized classical form may be rewritten as

$$\frac{1}{T_1} = 0.49 \frac{A_{\mathbf{Q}}^2}{\hbar^2} \frac{1}{\Gamma} \frac{1}{(1+f_{NQR}^2/\Gamma^2)} \frac{(T/2\pi\rho_s)^2}{(1+T/2\pi\rho_s)^2}, \tag{12}$$

where $f_{NQR} = 18$ MHz and we assume that the spin dynamics follow the Lorentz form in the renormalized classical regime. This function is now double valued in Γ, which, in addition to signal wipeout, makes the determination of Γ in the region 5–35 K difficult. In that region, $\Gamma \sim f_{NQR}$, which implies fast relaxation and signal wipeout. From T_1 measurements alone it is impossible to know how much of the distribution of Γ is greater or less than f_{NQR}. All we can say for certain is that experimentally the value of $1/T_1$ is underestimated because the fastest sections are not observable. However, at 350 mK these difficulties disappear because all of the

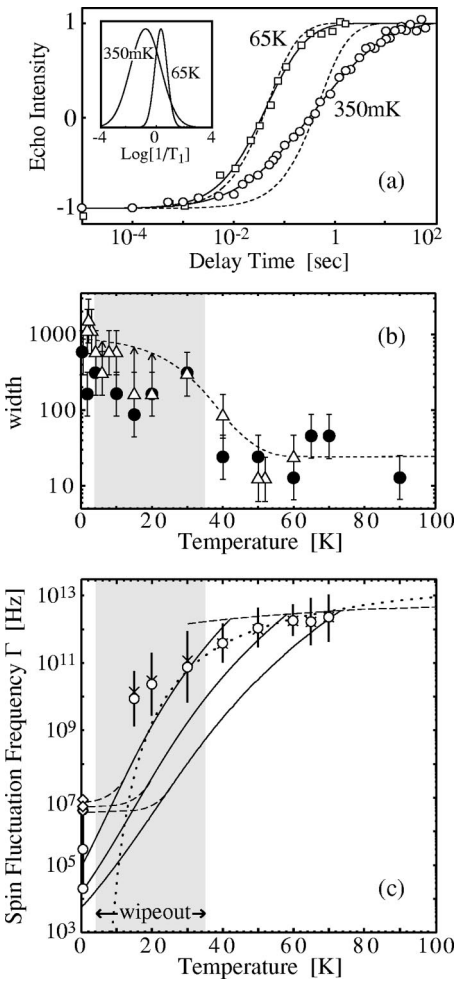

FIG. 12. (a) ^{139}La NQR recovery data at 350 mK and 65 K for $La_{1.68}Eu_{0.20}Sr_{0.12}CuO_4$ fit to single values of T_1 (dashed curves) and to distributions of T_1 (solid curves) as given in the inset (Ref. 71). The widths w of the distributions (defined as the quotient of the two T_1 values at the half maximum positions of the distributions) are plotted as a function of temperature in (b) for $La_{1.875}Ba_{0.125}CuO_4$ (△) and $La_{1.68}Eu_{0.20}Sr_{0.12}CuO_4$ (●). We note that the width is underestimated during NQR signal wipeout (the shaded region) and with this in mind we draw small vertical arrows from the most affected measurements and a dotted curve as a guide for the eye. In (c) the fluctuation frequency Γ deduced from T_1 [from a forced fit with single T_1, (×); central value of best fit distribution (○) with FWHM as given by the vertical bars]. At 350 mK we display data from a Lorentzian extension (○) of the form of T_1 and from a Gaussian extension (◇) (central value and FWHM positions marked with matching symbols for clarity). The solid and dashed curves are reproduced from Fig. 10(b) and act as guides for the eye and the dotted curve represents the form $\exp(-2\pi\rho_s^{eff}/T)$ with $2\pi\rho_s^{eff} = 200$ K.

signal intensity is recovered and we know that $\Gamma < f_{NQR}$. We can now safely employ Eq. (12) to determine the distribution of spin fluctuation frequencies, which is centered at 3×10^5 Hz with a width of more than two orders of magnitude.

In the preceding analysis for $\Gamma \lesssim f_{NQR}$ we chose to extend the RC form of $1/T_1$ with a factor of $1/(1+f_{NQR}^2/\Gamma^2)$ [Eq. (12)]. This assumption is certaintly justified for the paramagnetic spin dynamics above 70 K where the neutron data[45] fits well to a Lorentzian. However, there is no reason to believe that the very slow dynamics in spin stripes at 350 mK has to be governed by the same type of relaxational mechanism. For instance, if scattering by meandering hole rivers takes over as the dominant mechanism of spin fluctuations at low temperatures, the form of the relaxation function may change. Let us try another sensible choice, the form based on Moriya's Gaussian approximation,[80] which would give a frequency dependence on $1/T_1$ as

$$\frac{1}{T_1} = 0.49 \frac{A_{\mathbf{Q}}^2}{\hbar^2} \frac{1}{\Gamma} \exp\left[-\frac{f_{NQR}^2}{2\Gamma^2} \right] \frac{(T/2\pi\rho_s)^2}{(1+T/2\pi\rho_s)^2}. \qquad (13)$$

We also employ the form to deduce Γ at 350 mK, and find a much narrower distribution centered at a higher frequency, 5×10^6 Hz. We will discuss the implications of choosing either the Lorentzian or Gaussian form of $1/T_1$ in Sec. IV E. We note that in simulating the T_1 recovery curve we continue to employ Eq. (11) even for Γ close to and less than f_{NQR}. In that region the spectral function is not flat over the three resonant transitions, invalidating the basis of Eq. (11). Continued use of Eq. (11) is justifiable because the distribution in $^{139}1/T_1$ extends over several orders of magnitude and should be much greater than the potential error induced through the continued use of Eq. (11).

D. Numerical simulations of NQR signal wipeout and recovery, neutron, and μSR measurements

As previously defined, wipeout is the amomalous loss of NQR signal intensity. For $La_{2-x-y}(Nd,Eu)_ySr_xCuO_4$ with $0.12 \approx \frac{1}{8}$, the onset temperature T_{NQR} (Ref. 81) of the ^{63}Cu NQR wipeout agrees very well with the onset temperature T_{charge} of short-range charge order detected by neutron [2,7–9,22] and x-ray scattering measurements.[17,18] Moreover, the fraction of wipeout $F(T)$ shows a characteristic temperature dependence which is nearly identical to the charge order parameter observed by scattering techniques (i.e., the square root of the scattering intensity of the charge order peak), leading us to argue that the temperature dependence of the wipeout fraction $F(T)$ is a *good measure*[10] of the charge order parameter. Recent ^{139}La NMR studies of $La_2NiO_{4+\delta}$ by Abu-Shiekah *et al.*[82] also showed that the temperature dependence of the wipeout fraction of ^{139}La NMR in a high magnetic field (with an onset temperature of ~ 200 K) agrees quite well with the charge stripe order parameter[83] observed by elastic neutron scattering by Tranquada and co-workers.[84,85]

Naively thinking, the slowing charge fluctuations can make *direct* contributions to wipeout through extreme NQR line broadening similar to the case of conventional CDW systems[86–88] and also through extremely fast quadrupole relaxation times.[41,42] It is difficult to access how strongly the charge fluctuations near T_{charge} affect the NQR properties of the missing signals because the signals from the already stripe-ordered segments are not observable, similar to the *all or nothing* behavior of wipeout observed for Cu:Mn.[89]

In addition to the direct charge contribution to wipeout, we have also pointed out that *charge order turns on low-frequency spin fluctuations* below T_{NQR} within the charge-ordered domains, which in turn causes wipeout by making $^{63}T_1$ and $^{63}T_2$ too short to detect the ^{63}Cu NQR spin-echo signal.[10] That is, even if charge fluctuations are not strong enough to cause the wipeout of ^{63}Cu NQR directly, charge order creates patches of the CuO_2 plane that behave similarly to conventional spin glasses at slow time scales. As already noted by Hunt *et al.*,[10] dilute magnetic moments in metals [e.g., Cu:Fe (Ref. 90)] are known to cause wipeout of the NMR signal of the host metal. Restating this, we can say that the slowing charge dynamics is the *indirect* cause of ^{63}Cu NQR wipeout by triggering the drastic slowing of spin fluctuations within the regions where holes are trying to form charge rivers. Unfortunately, these important statements from Hunt *et al.* and Singer *et al.*[11] regarding the effects of strong spin dynamics on wipeout have been overlooked by some readers, including the authors of a recent publication from Los Alamos.[12]

Hunt *et al.* cited several pieces of experimental evidence that are consistent with the picture that anomalous slowing of spin dynamics are caused by slowing charge dynamics. First, inelastic neutron scattering measurements conducted at low energy transfers (1.75–3.5 meV) seem to show an anomalous enhancement of the low-frequency spin fluctuations near and below T_{charge}, even before quasielastic neutron scattering with energy transfer less than 1 meV detects frozen spins.[9]

Second, the spin-lattice relaxation rate $^{139}1/T_1$ at the ^{139}La sites begins to exhibit an anomalous upturn below T_{NQR}. This enhancement of $^{139}1/T_1$ is followed by a roughly exponential divergence at lower temperatures, $^{139}1/T_1 \sim \exp(2\pi\rho_s^{eff}/k_BT)$, where $2\pi\rho_s^{eff}$ is the effective spin stiffness which is of the order 10^1–10^2 K, as already shown by earlier comprehensive ^{139}La NQR measurements by Cho and co-workers in underdoped $La_{2-x}Sr_xCuO_4$.[36,37] Recalling that the exponential divergence of $1/T_1$ is a typical signature of the low-temperature *renormalized classical scaling* behavior of $S=\frac{1}{2}$ quantum Heisenberg systems in both isotropic[91,56] and anisotropic 2D systems,[72] the exponential divergence of $^{139}1/T_1$ below T_{NQR} is consistent with a rather drastic reduction of the effective spin stiffness ρ_s^{eff} caused by slowing charge dynamics. The spin-spin correlation length measured by Tranquada *et al.* also supports the renormalized, small spin stiffness with $2\pi\rho_s^{eff} \approx 200$ K.[9] In contrast, we recall that the fundamental energy scale in hole-doped $La_{2-x}Sr_xCuO_4$ is set by $2\pi\rho_s \approx 1730$ K as shown by NQR (Refs. 56 and 73 and neutron scattering.[92] High-energy scales of the order of 600 K are also inferred from a scaling analysis of the uniform spin susceptibility by Johnston[93] and

Hwang *et al.*[94] This suggests that a drastic reduction in spin fluctuation energy scales of the order of 10^3–10^2 K occurs near the charge ordering temperature. This has an important consequence on the wipeout phenomenon, because quite generally the overall magnitude of nuclear relaxation rates $^{63}1/T_1$ and $^{63}1/T_2$ are inversely proportional to the spin fluctuation energy scale $^{63}1/T_{1,2} \propto 1/2\pi\rho_s^{eff}$.[78] The observed relaxation rate $^{63}1/T_1 \sim 2000$ sec^{-1} is quite fast even above T_{charge} in hole-doped high-T_c cuprates, while ^{63}Cu NQR signals become unobservable when relaxation rates exceed $^{63}1/T_1 \sim 6000$ sec^{-1} for measurements with the quantization axis along the crystalline c axis.[56] When $^{63}1/T_1$ exceeds ~ 6000 sec^{-1} the relaxation times $^{63}T_1$ and $^{63}T_2$ become shorter than the limit of experimentally accessible times. In other words, the ^{63}Cu NQR signal in *all* high-T_c cuprates is on the verge of wipeout due to strong low-frequency spin fluctuations. This means that a factor of 2–3 reduction in spin stiffness ρ_s^{eff} near T_{charge} caused by slowed charge dynamics would immediately wipe out ^{63}Cu NQR signals. This explains why the ^{63}Cu NQR wipeout fraction accurately tracks the charge order parameter as measured by scattering experiments if one interprets the latter as a measure of the volume fraction of charge-stripe-ordered segments.

Third, the Gaussian component of spin-spin relaxation process $^{63,65}1/T_2$ at the ^{63,65}Cu sites crosses over to Lorentzian (single-exponential) decay below T_{charge} by motional narrowing effects due to fluctuating magnetic hyperfine fields.[10,11] The dominance of spin rather than charge fluctuations in the mechanism of the Lorentzian spin-echo decay was suggested by the isotope ratio between ^{63,65}Cu.[10,11] This crossover of spin-echo decay, accompanied by NQR/NMR intensity wipeout, is known to be a typical signature of the slowing down of conventional spin-glass systems such as Cu:Mn.[89,95] Thus all of these results as well as the dramatic increase in the EPR linewidth[16] are consistent with a simple picture that spin-glass-like behavior sets in when charge dynamics slow down, and the combined effects of slowing charge and spin stripe fluctuations can naturally provide a qualitative account of the wipeout behavior for $x \gtrsim \frac{1}{8}$ below $T_{NQR} \approx T_{charge}$.

In a recent article, Curro and co-workers[12] made an important observation that enabled a quantitative estimation of the *indirect* spin contribution to wipeout.[10,11] The essence of the analysis of Curro and co-workers is as follows. First, instead of saying that *extremely short* $^{63}T_1$ *and* $^{63}T_2$ *result in wipeout*,[10,11] they note that the ^{63}Cu *NQR signal cannot be detected if* $^{63}T_1$ *and* $^{63}T_2$ *are shorter than certain cutoff values labeled* $^{63}T_1^{critical}$ *and* $^{63}T_2^{critical}$. Using several assumptions, they estimate these cutoff values. Once $^{63}T_1^{critical}$ is deduced, Curro *et al.* use the Bloembergen, Purcell, and Pound (BPP) form[42] of T_1 to determine the corresponding spin fluctuation frequency $^{63}\Gamma^{wipeout}$. The wipeout fraction is the weight of the spin fluctuation distribution that is slower than $^{63}\Gamma^{wipeout}$ because the slower segments have $^{63}T_1$ and $^{63}T_2$ that are too fast to allow the detection of the spin echo.

Inspired by their analysis, we attempt to fit not only the wipeout of the ^{63}Cu NQR signal below $T_{NQR} \approx 70$ K but also its recovery below 8 K, the wipeout of ^{139}La NQR signal below 40 K and its recovery below 18 K, the spin order parameter measured by elastic neutron scattering below 50 K, and the μSR asymmetry below 30 K by taking into account the qualitative change in spin dynamics below T_{charge}.

We take the following approach, which relies primarily on experimental data instead of theoretical assumptions. In order to set $^{63}\Gamma^{cutoff}$ we note that $^{63}1/T_1 \approx 2000$ sec^{-1} at 70 K, at which temperature we know that the energy scale of spin fluctuations is $h\Gamma \approx 15$ meV from neutron scattering. From earlier ^{63}Cu NQR studies in paramagnetic La_2CuO_4,[56] we empirically know that the loss of ^{63}Cu NQR intensity due to fast relaxation occurs when the relaxation rate exceeds $^{63}1/T_1^{critical} \approx 6000$ sec^{-1}. Following Eq. (10), this implies that $^{63}\Gamma^{wipeout}$ is approximately a factor of 3 lower than the value of $h\Gamma \approx 15$ meV at 70 K. In this way, we define $^{63}\Gamma^{wipeout} \equiv 5$ meV, which is 1.2×10^{12} Hz (so that $1/^{63}\Gamma^{wipeout} \approx 0.83$ psec).

The cutoff for the wipeout of ^{139}La NQR signal is found in an analogous manner. From our experiments shown below in Fig. 16 and Fig. 17, we see that $^{139}1/T_1$ rises to approximately 80 sec^{-1} when wipeout is most severe. The remaining portion of the sample is on the verge of wiping out and has T_1 very close to $^{139}1/T_1^{critical}$. Thus we take $^{139}1/T_1^{critical} \equiv 80$ sec^{-1}. We now need to convert this value of $^{139}1/T_1^{critical}$ to the corresponding frequency scale. Using the renormalized classical form [Eq. (10)] in the high-frequency limit ($\Gamma \gg \omega_n$) we see that

$$\frac{1}{T_1} \propto \frac{(\gamma_n H_{hf})^2}{\Gamma} \frac{(T/2\pi\rho_s)^2}{(1+T/2\pi\rho_s)^2}, \tag{14}$$

where wipeout occurs at 70 K for ^{63}Cu and at 40 K for ^{139}La, and we take $2\pi\rho_s \approx 200$ K as determined above. Since we know the ratio of the gyromagnetic ratios to be $^{139}\gamma_n/^{63}\gamma_n = 0.533$ and the ratio of the hyperfine fields at the two nuclear positions to be $^{139}H_{hf}/^{63}H_{hf} = 0.012$ as inferred from Zeeman-perturbed NQR in La_2CuO_4,[63,50] we immediately calculate $^{139}\Gamma^{wipeout} = 5.1\times10^8$ Hz. We note that the $^{139}F(T)$ data are taken with a fixed delay time $\tau = 40$ μsec, which is justified due to the slow relaxation rate $^{139}1/T_2$ at the La site (see the inset of Fig. 16).

At low temperatures, the ^{63}Cu and ^{139}La NQR signal that was wiped out begins to reemerge. The return of signal begins at about 8 K for ^{63}Cu and 18 K for ^{139}La. Within our model, the reemergence of signal is not surprising; in fact, it is to be expected if the frequency range falls low enough so that T_1 and T_2 become longer. Using the Lorentzian extension of the renormalized classical form [Eq. (12)], with the NQR resonance frequency f_{NQR} taken as 6 MHz and 35 MHz for ^{139}La and ^{63}Cu, respectively, that the relaxation rate $1/T_1$ achieves its maximum value when the characteristic fluctuation frequency Γ coincides with f_{NQR}. Below that, additional slowing of the fluctuations (decreasing of Γ) reduces the relaxation rate $1/T_1$, so that at some low-frequency scale, which is defined as $\Gamma^{recovery}$, the following condition is satisfied: $1/T_1(\Gamma^{recovery}) = 1/T_1(\Gamma^{wipeout}) = 1/T_1^{critical}$ where we include temperature factors from Eq. (14). We note

that $\Gamma^{recovery} < f_n < \Gamma^{wipeout}$. Within this model, it is straightforward to deduce that $^{139}\Gamma^{recovery} = 2.9 \times 10^5$ Hz and $^{63}\Gamma^{recovery} = 4.0 \times 10^4$ Hz. This means that the slowest components within that sample slow to 2.9×10^5 Hz at approximately 18 K, providing ^{139}La NQR signal recovery, and continue to slow through 4.0×10^4 Hz at 8 K where they are manifested as recovered the ^{63}Cu NQR signal.

Combining all of these pieces of information regarding the spin fluctuation time scales in the stripe phase, we construct a chart showing the anchoring points of the temperature dependence of spin fluctuation frequency scale Γ, as presented in Fig. 10(b). Using these anchoring points, we smoothly interpolate to define a single distribution function $D(T,f)$, which gives the relative fraction of the sample volume that experiences fluctuations at frequency f at temperature T. This distribution is depicted by the black and gray contours in Fig. 10. We begin with an educated guess of the form of the distribution function, and refine the function as we iteratively produce a better and better fit to the experimental data as presented throughout this section. In this way we deduce the actual fluctuation spectrum based on the experimental data. Since there are no experimental constraints for Γ in the range above $^{63}\Gamma^{wipeout}$ but less than the ω/T scaling line, we are forced to extrapolate in that region. In Fig. 10 we depict the smooth extrapolations of $D(T,f)$ that terminate at the ω/T scaling line at a temperature above T_{charge}. However, we note that we are ignoring the possible contribution of the slowing of charge dynamics to Cu NQR wipeout effects.

The simulated wipeout fraction $F(T)$ is the fraction of the NQR signal that is not observable, which corresponds to the portion which experiences fluctuations that are slower than $\Gamma^{wipeout}$ but faster than $\Gamma^{recovery}$. This can be written as

$$F(T) = \frac{\int_{\Gamma^{recovery}}^{\Gamma^{wipeout}} D(T,f)df}{\int_0^{\infty} D(T,f)df}, \tag{15}$$

where the denominator acts as a normalization condition on $D(T,f)$ at every temperature. For the neutron scattering and μSR measurements, the fraction of the sample that has ordered is given by a similar form

$$G^{probe}(T) = \frac{\int_0^{\Gamma^{probe}} D(T,f)df}{\int_0^{\infty} D(T,f)df}, \tag{16}$$

where $probe$ is either μSR or $neutron$.

All four of these quantities [$^{63}F(T)$, $^{139}F(T)$, $G^{neutron}(T)$, and $G^{\mu SR}(T)$] have been numerically computed over a range of temperatures using the distribution $D(T,f)$ presented in Fig. 10(b), and the resulting curves are plotted in Fig. 13 along with the relevant experimental data. The simulations work remarkably well in reproducing both the ^{63}Cu and ^{139}La wipeout data, as well as the neutron and μSR results. As mentioned previously, the quality of these fits is the result of iterative alterations of trial distribution functions that eventually led us to the distribution $D(T,f)$ shown in Fig. 10(b). We find that a distribution function based on a Gaussian in $\log f$ with different widths to higher and lower frequency works well. However, the use of an iterative method means that we cannot exclude the possibility that a somewhat different f and T dependence of $D(T,f)$ may work as well as this one, although it is difficult to imagine that a qualitatively different form would succeed, given the large number of experimental constraints that must be satisfied.

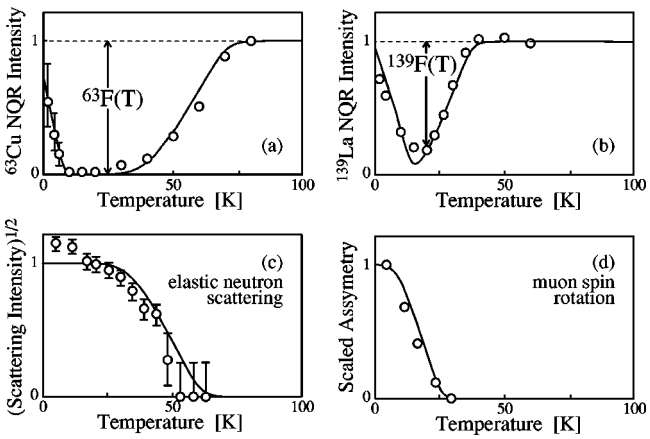

FIG. 13. Four sets of experimental data and corresponding numerical simulations based on the model described in the text, using the $D(T,f)$ shown in Fig. 10(b). (a) ^{63}Cu wipeout in $La_{1.68}Eu_{0.2}Sr_{0.12}CuO_4$, (b) the ^{139}La wipeout from the $|\pm\frac{1}{2}\rangle \leftrightarrow |\pm\frac{3}{2}\rangle$ transition in $La_{1.68}Eu_{0.2}Sr_{0.12}CuO_4$. (The wipeout behavior at $x \approx \frac{1}{8}$ is nearly identical for Eu-, Nd-, and Ba-codoped samples.) (c) The spin order parameter in $La_{1.48}Nd_{0.4}Sr_{0.12}CuO_4$ deduced from elastic neutron scattering as the square root of the scattered intensity, from Tranquada *et al.*, (Ref. 2) and (d) the μSR asymmetry factor $A_{\perp}/A_{total} \times \nu^2$ in $La_{1.475}Nd_{0.4}Sr_{0.125}CuO_4$ from Nachumi *et al.* (Ref. 29).

Although we do not explicitly utilize the nuclear spin-lattice relaxation rate $1/T_1$ in the analysis of this section, our choice of the form of T_1 for Γ below the Larmor frequency does play an important role in setting the vertical position of the anchoring points in Fig. 10. To this point we have utilized the Lorentzian form [Eq. (12)], but as discussed in Sec. IV C, we might do better to employ the Gaussian form [Eq. (13)]. Although this change does not alter any of the analysis for $\Gamma > 5 \times 10^7$ Hz, it does substantially change the behavior for smaller Γ. Specifically, the cutoff frequencies for the recovery of both ^{63}Cu and ^{139}La NQR signals are shifted upwards to $\sim 5 \times 10^6$ Hz, causing the distribution $D(T,f)$ to saturate at low temperatures as shown by the dashed curves in Fig. 10(b) and in Fig. 12. We will discuss the merits of the Gaussian form of $1/T_1$ in Sec. IV E.

E. Summary of fluctuation time scales and comparisons to related works

Through an analysis of both the $^{139}1/T_1$ recovery data and the ^{63}Cu and ^{139}La wipeout data we arrived at two estimates of the spin fluctuation spectra as a function of temperature as

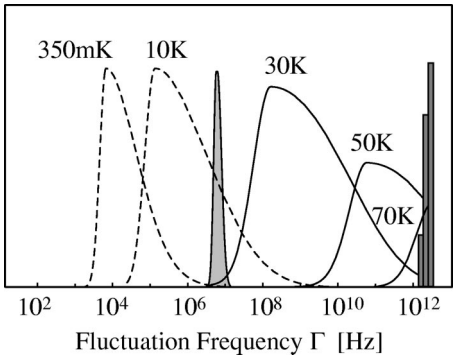

FIG. 14. Slices of the frequency distribution $D(T,f)$ as deduced from the analysis of Sec. IV D (Ref. 71). The shaded rectangles represent the spectral weight in the sharply defined ω/T energy scale (70 K is the rightmost, 50 K in the center, and 30 K at the left), which decreases in magnitude at lower temperature as the spectral weight is shifted to the contribution from the stripe-ordered regions represented by the broad curves. The dashed curves arise from a Lorentzian extension of the form of T_1 [Eq. (12)] and the shaded curve corresponds to a Gaussian extension [Eq. (13)] at 350 mK.

shown in Figs. 10(b) and 12. As an alternative presentation of the data in Fig. 10(b), we construct Fig. 14, which contains slices through the distribution $D(T,f)$ at selected temperatures. We find that there is a sharp change from the high-temperature ω/T-dominated behavior to the much faster exponential slowing of spin fluctuations below T_{charge}. We understand this qualitative change in the magnetic fluctuation spectrum to be due to charge ordering. The two methods of deducing Γ are in qualitative agreement, even though the quadrupole contribution to relaxation and wipeout makes the approach based on $^{139}1/T_1$ somewhat questionable. The differences between the two methods are smaller than the effects of choosing a Lorentzian or Gaussian extension of the form of T_1. Without additional information we would be able to proceed no further—however, we know from the line shape analysis that our 350 mK line shape is still experiencing some motional averaging. In the Lorentzian schemes more than 50% of the distribution of Γ is lower than $\Gamma = 3 \times 10^4$ Hz, which corresponds to 30 μsec, the duration of a pulsed NQR experiment. This indicates that motional averaging is unlikely to be effective for the bulk of the sample and we would expect to see frozen structures in the low-temperature Zeeman-perturbed spectra, which are not observed. However, using a Gaussian model we find that almost all of the sample experiences fluctuations faster than the experimental duration, indicating the likelihood of strong motional averaging. Thus, reality is closer to the Gaussian form in order to preserve motional averaging. We also note that the low-temperature saturation of Γ that naturally arises from the aforementioned analysis within the Gaussian form is consistent with the saturation of the spin-spin correlation length observed below 20 K.[9]

Before continuing, we point out some qualitative similarity between $D(T,f)$ for the present case of the striped cuprates below T_{charge} and for the conventional spin-glass system Cu:Mn investigated by Murani by cold neutron scattering studies.[96] It is also important to note that at the slow time scales of NQR, the striped phase never looks to be striped, but rather behaves more or less like a conventional spin glass. This similarity with the cluster spin-glass phase has been repeatedly emphasized by Borsa and co-workers[36,37,91] since before the discovery that the spin-glass phase is actually striped by neutron scattering.[2–8] However, we note that the striped phase does differ from conventional spin glasses, even at slow time scales. Specifically, we point out that the real part of the susceptibility shows only small Curie enhancement, indicating the scarcity of free spins. In fact, comparing $La_{1.87}Ba_{0.13}CuO_4$ (Ref. 97) and Zn-impurity-doped $La_{1.85}Sr_{0.15}Cu_{0.98}Zn_{0.02}O_4$ (Ref. 98) where 2% of the moments are intentionally made to be free, we find that the Curie component of the susceptibility is nearly two orders of magnitude smaller in the Ba-doped material below T_{charge} than in the Zn-doped case. This implies that the number of free spins in $La_{1.87}Ba_{0.13}CuO_4$ is very small. It is more likely that the spin-glass-like behavior is caused by slow fluctuations of self-organized, short-range-ordered segments with spin and charge density modulation.

Recently, Curro *et al.*[12] and Teitel'baum *et al.*[68] have reported methods of simulating the wipeout effects. In both cases the authors attribute ^{63}Cu NQR signal wipeout to slowing spin fluctuations. We emphasize that the importance of slowing spin fluctuations on NQR signal wipeout through the extremely large relaxation rates $^{63}1/T_1$ and $^{63}1/T_2$ (the *indirect* contribution) has already been discussed repeatedly in our earlier publications.[10,11] The contribution of Curro and co-workers is in the introduction of a numerical cutoff to fit wipeout effects, making quantitative analysis possible.[12] Their pioneering work opened a path to gain quantitative information regarding the distribution of the spin fluctuation frequency Γ. This is an important idea that is applicable to the analysis of various NMR data and they should be fully credited for their contribution. However, Curro *et al.* overlooked the fact that the importance of spin fluctuations to wipeout (the *indirect* contribution) had originally been proposed by us and quoted our publications only in the context of slowing charge dynamics. We believe that this inaccurate quotation is misleading at best. Even though they have implied that their way of understanding the wipeout effects was entirely novel, we must emphasize that the physical processes utilized in their analysis have little difference from the ideas outlined in Hunt *et al.* regarding the *indirect* process, except for one crucial point. We believe that the onset of charge order (or slowing of charge dynamics for $x \lesssim \frac{1}{8}$ due to random localization effects[11]) is the cause of the drastic changes in the magnetic properties that result in NQR signal wipeout. On the other hand, in the analysis of Curro and co-workers it is *assumed* that glassy slowing of Cu spin fluctuations continuously proceeds from 300 K to 4 K without any qualitative changes in spin dynamics through T_{charge}. That is, Curro *et al.* assume that the same activation temperature dependence of $\Gamma(T) \propto \exp(-E_a/k_BT)$ properly represents the slowing of Cu spin fluctuations both above and below T_{charge}. They fit $^{139}1/T_1$ below 30 K ($< T_{charge}$) to deduce the activation energy E_a and its distribution Δ. Ignoring the drastic change in the charge degree of freedom near T_{charge}

and the resulting changes in spin dynamics as reflected in $^{139}1/T_1T$, electron paramagnetic resonance (EPR)[16] etc., these parameters are taken to remain unchanged even above T_{charge}.

We note several inconsistencies arising from the assumptions of the Los Alamos group. We point out that the fit of $^{139}1/T_1$ by Curro and co-workers fails on their own data set above 30 K. In addition, within the model of Curro *et al.*, $^{63}1/T_1$ has the same Gaussian distribution as $\Gamma(T)$ with the same activation-type temperature dependence $^{63}1/T_1 \propto \exp(E_a/k_BT)$, which is taken to hold for all temperatures. Unfortunately, this assumed exponential *increase* of $^{63}1/T_1$ is in sharp contradiction with the experimental finding that $^{63}1/T_1$ *decreases* with decreasing temperature down to T_{charge} as shown in Fig. 11. We note that the assumed exponential form above T_{charge} is essentially equivalent to extrapolating $^{63}1/T_1$ along the dotted lines of Fig. 11 between T_{charge} and 300 K. Thus, there is no justification for the assumed forms of $\Gamma(T)$ and $^{63}1/T_1$ above T_{charge}. Since the calculated wipeout fraction by Curro *et al.* relies on the exponential temperature dependence of $^{63}1/T_1$, we must conclude that qualitative success in reproducing wipeout starting at as high as 150 K is merely a coincidence that depends strongly on their choice of $^{63}\Gamma^{wipeout}$.

Finally, although we believe that the slowing of charge dynamics is of extreme importance and that the analysis of the Los Alamos group is not applicable for $x \gtrsim \frac{1}{8}$, we note that their assumed form of $\Gamma(T)$ is similar to our finding for $x=0.07$ below T_{NQR}. However, we note that in this region the beginning of charge localization has been observed by Ichikawa *et al.* at $\sim T_{NQR}$.[22] (See Sec. V C for a discussion of the underdoped materials.) Hence, one may consider the slowing of charge dynamics as the cause of the glassy slowing of spin fluctuations regardless of spatial coherence, which is gradually lost with decreasing x.[10,11]

After an early version of this work was presented elsewhere,[99] NQR wipeout was also simulated by a group at Leiden University[68] who have independently pointed out that ^{139}La NQR intensity provides valuable information regarding Γ. They base their analysis on ^{139}La spin-lattice relaxation data in Nd-codoped materials. Although we agree that $^{139}1/T_1$ is a good place to initiate a study of the fluctuation spectrum and Cu wipeout, we note that nuclear relaxation in Nd-codoped materials is usually dominated by the large Nd moment, as in $NdBa_2Cu_3O_7$,[100] and $Nd_{2-x}Ce_xCuO_4$.[101] This also seems to be the case in Nd-doped $La_{2-x}Sr_xCuO_4$ as shown in Fig. 17. Furthermore, we find that $^{139}1/T_1$ in Nd-codoped materials is roughly independent of hole doping.[102] Bearing this in mind, it seems that their analysis would then predict identical wipeout for different hole concentrations x, which is certainly not the case (see Fig. 15).

V. Nd- AND Eu-CODOPED MATERIALS AWAY FROM $x \approx \frac{1}{8}$

A. Construction of a unified phase diagram

Now that we have reached a good quantitative understanding of the spin stripe fluctuations and its temperature dependence for the magic hole concentration of $x \approx \frac{1}{8}$, we seek a comprehensive understanding of stripe fluctuations across the entire phase diagram of $La_{1.6-x}Nd_{0.4}Sr_xCuO_4$ and $La_{1.8-x}Eu_{0.2}Sr_xCuO_4$. The temperature dependences of the ^{63}Cu NQR wipeout $^{63}F(T)$, ^{139}La NQR intensity, and $^{139}1/T_1T$ are presented in Figs. 15, 16, and 17, respectively. Utilizing this information, as well as available elastic neutron scattering and μSR measurements, we follow the analysis of Sec. IV D to deduce the temperature dependence of the spin fluctuation spectrum Γ for hole concentrations of $x=0.07,0.12,0.16$, and 0.20. The results are depicted in Fig. 10 together with the simulated ^{63}Cu wipeout.

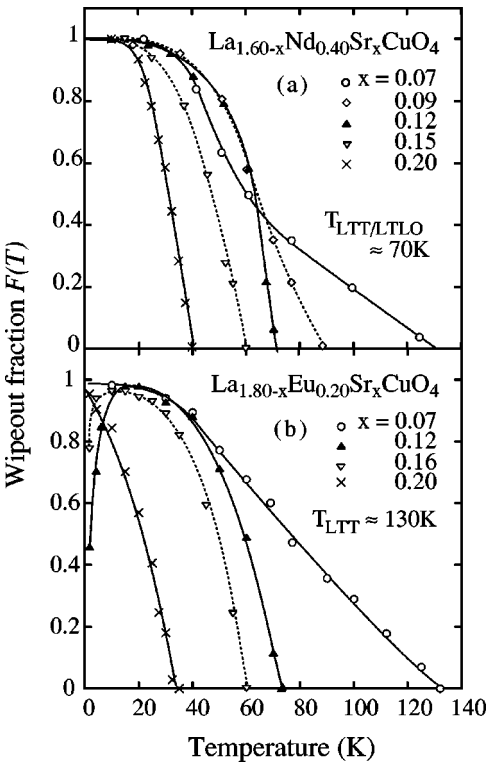

FIG. 15. (a) The fraction of wiped-out signal, $^{63}F(T)$, in $La_{1.6-x}Nd_{0.4}Sr_xCuO_4$. The low-temperature structural phase transition temperature T_{LTT} at $x \approx \frac{1}{8}$ is $T_{LTT} \approx 70$ K (Ref. 22). The lines are guides for the eye and only data points below T_{NQR} are plotted. (b) is the same plot but for $La_{1.8-x}Eu_{0.2}Sr_xCuO_4$. At $x \approx \frac{1}{8}$, $T_{LTT} \approx 130$ K (Ref. 16).

Another way to illustrate the temperature dependence of the spin dynamics of stripes is to plot the contours of characteristic frequency scales on the temperature (T) versus hole concentration (x) phase diagram. In Fig. 18, we collect data from various experiments and plot the temperature at which each experimental probe experiences an anomaly. The anomaly occurs at the temperature at which the spin fluctuations of some parts of the CuO_2 plane slow to the inherent frequency of that probe. Using the anomaly temperatures as a boundary, we section off areas of the phase diagram into various shades of gray.

The white area at the top of the plot corresponds to the temperature region with very fast spin fluctuations, where stripes can be considered to be completely dynamic. In other words, this is the region where the so-called ω/T *scaling*

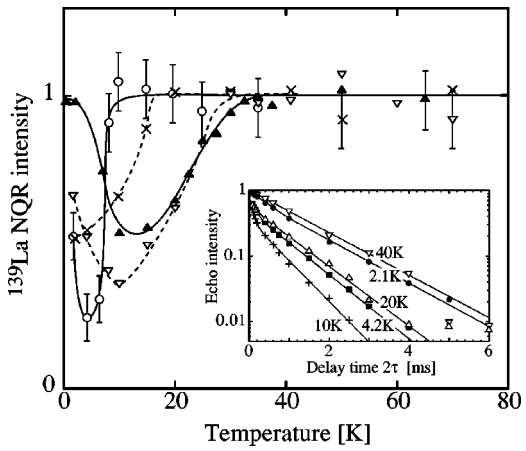

FIG. 16. Plot of the ^{139}La NQR signal intensity in $La_{1.8-x}Eu_{0.2}Sr_xCuO_4$ for the $|\pm\frac{5}{2}\rangle\leftrightarrow|\pm\frac{7}{2}\rangle$ transition at a frequency $3\nu_Q\approx 18$ MHz [$x=0.07$ (○), 0.12 (▲),0.16 (▽), 0.20 (×)]. The intensity was measured for a fixed pulse separation time of $\tau=40$ μsec. In the inset we show the spin-echo decay for $La_{1.68}Eu_{0.20}Sr_{0.12}CuO_4$ at different temperatures. All curves are guides for the eye.

holds for spin dynamics, and there is a well-defined spin fluctuation time scale whose distribution is minimal. (It should be noted that there is NMR evidence for some spatial inhomoginiety even in a similar high-temperature regime, as recently reported by Haase and co-workers on the basis of some ingenious NMR measurements and analysis,[103] and by a report of the frequency dependence of $^{63}1/T_1$ by Fujiyama *et al.*[104])

The darkest gray region shows where the spin fluctuations are so slow that the hyperfine field is nearly static even at the NQR times scales. This region is obtained based on the appearance of hyperfine broadening in the recovered NQR signals of ^{63}Cu. Between the lightest and darkest gray areas, which correspond to the wipeout and recovery of ^{63}Cu NQR signal, there are five separate regions depicted in Fig. 18. The boundary marked by solid circles is set by the temperature at which $^{139}1/T_1T$ crosses the value 0.05 sec^{-1} K^{-1} in $La_{1.8-x}Eu_{0.2}Sr_xCuO_4$ (see Fig. 17). $^{139}1/T_1T$ is somewhat larger at high temperatures for $x=0.20$, so in this case we use the temperature (25 K) at which the enhancement of $^{139}1/T_1T$ begins. The next boundary is set by T_{spin}, the onset of elastic neutron scattering from spin stripes corresponding to a frequency scale of 0.5–1.0 meV, based on the energy integration windows of those experiments. The next area marks the onset temperature of ^{139}La NQR wipeout. Open diamonds mark the onset temperature for muon spin rotation $T_{\mu SR}$ arising from static order on the time scales of μSR measurements.[29] At temperatures lower than 20 K the NQR signal begins to recover for the ^{139}La nuclei. These temperatures are marked by open, downward pointing triangles in Fig. 18. Also shown in Fig. 18 are the onset temperatures T_{charge} for short-range charge order as obtained from neutron scattering[22] and x-ray scattering,[17,18] the transition to the superconducting phase in $La_{1.6-x}Nd_{0.4}Sr_xCuO_4$ (a white line), and a dotted black line (as a guide for the eye) that

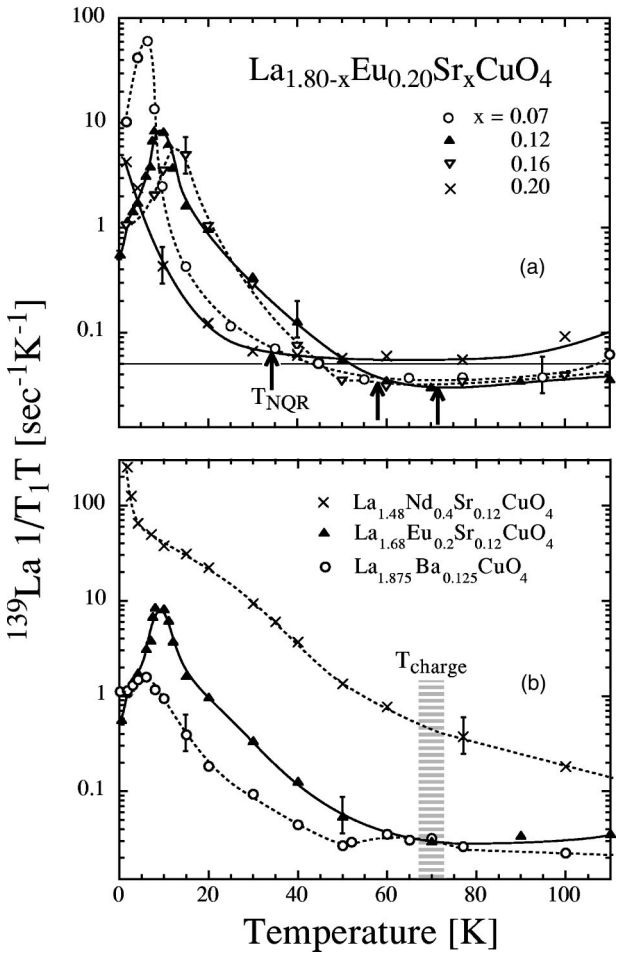

FIG. 17. (a) Plot of $^{139}1/T_1T$ of the $|\pm\frac{5}{2}\rangle\leftrightarrow|\pm\frac{7}{2}\rangle$ transition for the La site in $La_{1.8-x}Eu_{0.2}Sr_xCuO_4$ where the symbols used for each hole concentration x are listed in the figure. The horizontal line marks the constant $^{139}1/T_1T\approx 0.05$ sec^{-1} K^{-1} value and the arrows mark T_{NQR} for each material $x=0.20$, 0.16, and 0.12 from left to right. (b) The same quantity, for several samples with hole concentration $x\approx\frac{1}{8}$. Note that the Nd-codoped system has an enhanced relaxation rate due to the Nd moments. The bump in the data for the Ba-doped sample near 60 K arises from the low temperature tetragonal (LTT) structural transition.

follows T_{charge} and the Cu wipeout inflection points. The importance of the inflection points will be explained below.

B. Results for $x\gtrsim\frac{1}{8}$

We have already discussed the sharp onset of the slowing of spin fluctuations that occurs at T_{charge} for $x=0.12$ which is caused by charge order. Looking at the higher hole concentrations $x=0.16$ and 0.20, we see similar behavior in the ^{63}Cu NQR wipeout (Fig. 15), ^{139}La NQR wipeout (Fig. 16), and $^{139}1/T_1T$ (Fig. 17), although in each case the temperature scale is shifted increasingly downwards for the samples farther from the magic hole concentration $x\approx\frac{1}{8}$. This naturally leads to a similar distribution of Γ that is shifted to lower temperature, as shown in Figs. 10(c) and 10(d). In the case of $x=0.16$ we find that all of the anchoring points of the distribution are shifted to lower temperatures by $\sim$10 K

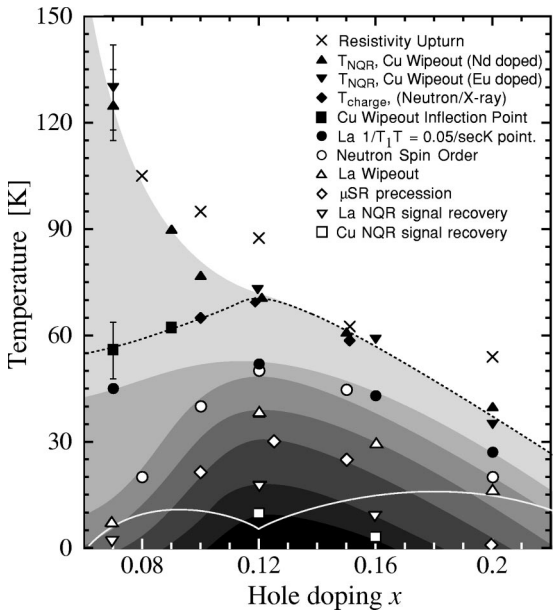

FIG. 18. Phase diagram for $La_{1.6-x}Nd_{0.4}Sr_xCuO_4$ and $La_{1.8-x}Eu_{0.2}Sr_xCuO_4$, showing the upturn in ab-plane resistivity temperature T_u found in $La_{1.6-x}Nd_{0.4}Sr_xCuO_4$ (Ref. 22) ($\times$), ^{63}Cu wipeout onset T_{NQR} in $La_{1.6-x}Nd_{0.4}Sr_xCuO_4$ ($\blacktriangle$) and $La_{1.8-x}Eu_{0.2}Sr_xCuO_4$ ($\blacktriangledown$), onset temperature T_{charge} for short range charge order according to neutron (Refs. 7 and 22) and X-ray (Refs. 17 and 18) in $La_{1.6-x}Nd_{0.4}Sr_xCuO_4$ ($\blacklozenge$), the copper wipeout inflection point ($\blacksquare$) in $La_{1.6-x}Nd_{0.4}Sr_xCuO_4$, the temperature where $^{139}1/T_1T=0.05$ sec^{-1} K^{-1} in $La_{1.8-x}Eu_{0.2}Sr_xCuO_4$ ($\bullet$), long-range spin order T_{spin} (Refs. 8 and 22) in $La_{1.6-x}Nd_{0.4}Sr_xCuO_4$ ($\circ$), onset of La wipeout for $La_{1.8-x}Eu_{0.2}Sr_xCuO_4$ ($\triangle$), onset of μSR coherent precession $T_{\mu SR}$ (Ref. 29) for $La_{1.6-x}Nd_{0.4}Sr_xCuO_4$ ($\diamond$), the onset of ^{139}La recovery of signal in $La_{1.8-x}Eu_{0.2}Sr_xCuO_4$ ($\triangledown$), and the onset of ^{63,65}Cu recovery of signal in $La_{1.8-x}Eu_{0.2}Sr_xCuO_4$ ($\square$). The darker gray tones indicate increasingly slow fluctuation time scales. We also show the superconducting boundary as a white line and a dotted line that connects T_{charge} and the Cu wipeout inflection points as a guide for the eye.

while for $x=0.20$ the shift is $\sim$20–30 K. The striking similarity of the shapes of $\Gamma(T)$ for $0.12\lesssim x\lesssim 0.20$ indicates that the fundamental physics of these systems is very similar. In each of these cases we consider charge order as the cause of the anomalous glassy slowing of spin fluctuations. With increasing hole concentration the tendency to charge order diminishes, causing the shift of Γ to lower temperatures for larger x.

The same strong similarities for the samples with $x\gtrsim\frac{1}{8}$ can also be seen in the phase diagram of Fig. 18. The lightest gray corresponds to the region where some segments of the CuO_2 plane experience spin fluctuations slower than $^{63}\Gamma^{wipeout}$, and the ^{63}Cu NQR signal begins to wipe out. For $La_{1.6-x}Nd_{0.4}Sr_xCuO_4$ with $0.12\lesssim x\lesssim 0.15$, the boundary agrees well with the onset of short-range charge order as observed by scattering methods.[7,17] We note that our wipeout studies of $La_{1.6-x}Nd_{0.4}Sr_xCuO_4$ were conducted[11] without knowledge of the more recent results from x-ray scattering by Niemöller *et al.* for $x=0.15$,[18] and the good agreement

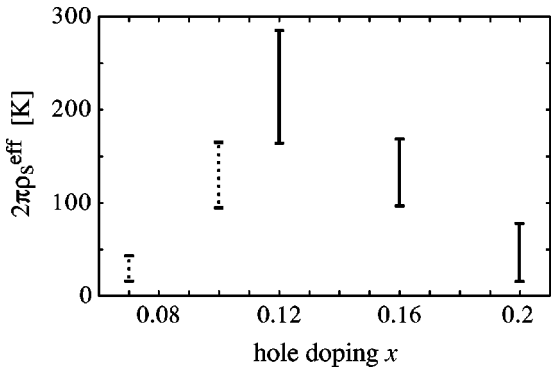

FIG. 19. Doping dependence of $2\pi\rho_s^{eff}$ as deduced from the data presented above in Fig. 18 by fitting to the form $\Gamma\propto\exp(-2\pi\rho_s^{eff}/T)$. We note that Γ levels for low temperature and that region are neglected in the fit, resulting in a large uncertainty in the value of $2\pi\rho_s^{eff}$. For $x<\frac{1}{8}$ tailed wipeout indicates that the physics may differ substantially from the region $x\gtrsim\frac{1}{8}$, so we use dashed lines in that region.

between our $T_{NQR}=60\pm5$ K and their $T_{charge}=55$ K strongly supports our indentification of T_{NQR} as the onset of the glassy slowing of the spin fluctuations triggered by slowing charge dynamics for $0.12\lesssim x\lesssim 0.15$. Generally speaking, for $x\gtrsim\frac{1}{8}$, we find that all of the contours are nearly parallel and slope downward with increasing x. Thus below the onset temperature for charge order T_{charge}, the slowing down is similarly rapid throughout this concentration range, but with an energy scale that decreases away from the magic doping level $x\approx\frac{1}{8}$ where the stripe fluctuations are most robust.[11] In fact, if we fit the slowing of spin fluctuations to the renormalized classical form $\exp(-2\pi\rho_s^{eff}/T)$ for different hole concentrations, we find that $2\pi\rho_s^{eff}$ decreases with increasing x above $x\approx\frac{1}{8}$ as shown in Fig. 19.

C. Results for $x\lesssim\frac{1}{8}$

Within the second region $x\lesssim\frac{1}{8}$, the slowing down is more gradual and the contours in Fig. 18 are more spread out. At this point it is worth pointing out that although T_{NQR} increases below $x\approx\frac{1}{8}$, $^{63}F(T)$ is more tailed as shown in Fig. 15 for $La_{1.6-x}Nd_{0.40}Sr_xCuO_4$ with $x=0.07$ and 0.09. It is important to note that there is an inflection point in the temperature dependence of the wipeout fraction, $^{63}F(T)$, at approximately 55 K and 62 K, respectively, for these two concentrations. In a recent study of a $La_{1.50}Nd_{0.4}Sr_{0.10}CuO_4$ single crystal provided by Ichikawa *et al.*, we confirmed[102] that this inflection point is nothing but the charge ordering temperature T_{charge} as determined by x-ray scattering.[22] The coincidence of T_{charge} and the low-temperature less orthorhombic (LTLO) structural phase transition temperature[22] may suggest that static one-dimensional charge order cannot develop without the tetragonal lattice symmetry that is compatible with the symmetry of charge stripes. The longer spatial coherence of charge order below T_{charge} accelerates wipeout at the inflection point. Even though static charge order with substantial spatial coherence has not developed between T_{NQR} and T_{charge}, transport measurements by

Ichikawa *et al.* show that the onset of wipeout agrees well with the temperature scale T_u for *local charge order* as deduced from a scaling analysis of the enhancement of in-plane resisitivity.[22] These results underscore the importance of the interplay between charge and spin degrees of freedom, even for $x \lesssim \frac{1}{8}$.

It would thus appear that for $x \lesssim \frac{1}{8}$, there is a precursive mechanism that wipes out the ^{63}Cu resonance signal below T_{NQR} before collective short-range charge order sets in at $T_{charge}(<T_{NQR})$. The nature of this precursive wipeout cannot be collective since there is no sharp onset, and thus cannot be explained in the terms discussed in Sec. IV. In earlier publications,[10,11] we have suggested that this precursive wipeout may be accounted for if we assume that individual holes begin to localize with decreasing temeprature, thereby creating local moments. This is a situation similar to the one that results in wipeout in conventional dilute Kondo alloys[90] and spin glasses[89,95] On the other hand, in this scenario in which the local moments are created by localization effects, the precursive wipeout may be further enhanced if one increases resistivity by introducing disorder. However, our recent experimental studies on Zn-doped $La_{2-x}Sr_xCuO_4$ show that the onset of wipeout T_{NQR} is a fairly well-defined temperature scale that does not vary even when resistivity is enhanced and local moments are introduced by Zn impurity doping.[102] Furthermore, a recent inelastic neutron scattering study[105] on a sample of $La_{1.93}Sr_{0.07}CuO_4$ showed a continual decrease of the fluctuation energy scale with decreasing temperature, followed by the freezing of spin stripes at low temperatures. The presence of a striped ground state indicates that it is unlikely that the glassy spin fluctuations below T_{NQR} have no spatially correlated stripe signature. We include data for $2\pi\rho_s^{eff}$ for the range $x<\frac{1}{8}$ in Fig. 19, but we reiterate the differences between the physics above and below $x \approx \frac{1}{8}$ and use dotted lines for the underdoped samples. We note that the trend of $2\pi\rho_s^{eff}$ decreasing away from $x \approx \frac{1}{8}$ is expected from the low-temperature behavior seen in Fig. 18, indicating that the relevant energy scale is indeed decreasing, even if an identical analysis is not entirely applicable.

VI. CONCLUSIONS

In this paper, we provide a comprehensive NQR picture of the spatial modulation and fluctuations of spin and charge density waves in the stripe phase of $La_{1.88-y}(Nd,Eu)_ySr_{0.12}CuO_4$ and $La_{1.875}Ba_{0.125}CuO_4$. From the analysis of the Zeeman-perturbed ^{63}Cu and ^{139}La NQR spectra, we deduce the spatial distribution of the hyperfine field at the time scales of NQR spin-echo measurements. We demonstrate that the maximum frozen Cu magnetic moment at 350 mK is relatively small, $\sim(0.1–0.2)\mu_B$, with a comparably large distribution. The fact that μSR studies find a large and well-defined effective moment of $\sim 0.3\mu_B$ at a time scale that is two orders of magnitude faster than NQR provides evidence that motional averaging is at least partially responsible for the supression of the effective moment as observed in our NQR measurements. Given that the mobility of holes in the CuO_2 planes at $T \ll T_{charge}$ is comparable to the metallic state,[21] perhaps it is reasonable that the magnitude of the frozen moment averaged over NQR time scales is fairly small and highly disordered, despite the fact that the spin-spin correlation length is known to reach ~ 200 Å below 30 K at neutron scattering time scales.[9] We also find that broadening of the quadrupole coupling is necessary to fit the low-temperature Zeeman-perturbed NQR line shape, indicating that there are spatial variations in the local charge state.

From a simple physical argument based on comparison of $^{139}1/T_1$ and the renormalized classical scaling of the O(3) nonlinear σ model, we show that the roughly exponential divergence of $^{139}1/T_1$ observed below T_{charge} is consistent with the presence of low-frequency spin fluctuations characterized by a reduced effective spin stiffness $2\pi\rho_s^{eff} \approx 200$ K. We attribute the renormalization of the spin stiffness from $2\pi\rho_s \sim 10^3$ K at higher temperatures to $2\pi\rho_s^{eff} \sim 10^2$ K to slowing charge dynamics that suppresses the Cu-Cu exchange interaction. By analyzing the magnitude and distribution of the nuclear spin-lattice relaxation rate $^{139}1/T_1$ based the nonlinear σ model with $2\pi\rho_s^{eff} \approx 200$ K, we deduce the spatial distribution of Γ (spin fluctuation frequency scale) of Cu below T_{charge}. We also analyze the ^{63}Cu and ^{139}La NQR wipeout fraction $F(T)$, elastic neutron scattering, and μSR data within the same framework, and obtain a nearly identical spectrum. Combined with the fact that only a small change of a factor of ~ 3 in the anomalous slowing of Γ is sufficient to account for the observed wipeout of ^{63}Cu NQR, this provides a natural explanation of why the temperature dependence of $F(T)$ tracks the charge order parameter measured by scattering techniques for $0.12<x<0.16$, which may be interpreted as the volume fraction of patches of the sample in which the spin fluctuations have started to slow exponentially. However, we note that our model is quite simpleminded, relying entirely on magnetic enhancement of $1/T_1$.[106] Fortunately, since the qualitative change in the temperature dependence of spin fluctuations from roughly T linear to exponential is so drastic, the overall picture of the temperature dependence of the spin fluctuation frequency scale Γ shown in Fig. 10 would not be substantially altered by a more elaborate analysis.

By plotting contours of spin fluctuation time scales in the T-x phase diagram, we demonstrate that a similar glassy slowing of stripes takes place away from the magic hole concentration $x=\frac{1}{8}$. However, we find a qualitative difference in the slowing between above and below $x=\frac{1}{8}$ where the measured incommensurability begins to saturate.[70] The origin of the difference is not well understood at this point. For $x<\frac{1}{8}$, a stronger tendency toward some sort of localized state seems to precede spatially periodic charge ordering,[21,22] probably inducing local spin-glass-like behavior with fairly high-temperature scales.[10,11,33] However, we emphasize that this spatially disordered spin-glass-like entity eventually freezes as stripes, as demonstrated by neutron scattering.[5] Hence T_{NQR} may be considered as the onset of the glassy freezing of stripes. A recent scaling analysis of resistivity data by Ichikawa *et al.*[22] suggests that this glassy freezing is triggered by a slowing charge dynamics, in support of our earlier proposal for the mechanism of wipeout and

glassy freezing.[11] We also believe that the qualitative difference above and below $x \approx \frac{1}{8}$ bears significant implications on the mechanism of superconductivity because the behavior of $La_{2-x}Sr_xCuO_4$ is very similar to $La_{1.88-y}(Nd,Eu)_ySr_{0.12}CuO_4$ at and below $x=\frac{1}{8}$, while the glassy freezing of stripes is not seen by NQR in superconducting $La_{2-x}Sr_xCuO_4$ for $x>\frac{1}{8}$.

Finally, we emphasize that the so-called stripe phase never looks striped at the slow time scales of NQR measurements even for $x \approx \frac{1}{8}$ at temperatures as low as 350 mK. It is certainly possible to argue that the segments of the CuO_2 plane in which the ^{63}Cu NQR signal is wiped out are very similar to a conventional spin glass, and at slow time scales those segments are phase separated from other patches of the CuO_2 plane where the Cu spins still behave as they did above T_{charge}. Whether such segments are fixed in space is not clear. The essence of the stripe physics is that these disordered patches of the CuO_2 planes with *slow* spin and charge dynamics appear striped if viewed by an experimental probe with a time scale that is faster than the remnant fluctuations.

ACKNOWLEDGMENTS

We thank many colleagues for sharing their wisdom with us, in particular J.M. Tranquada, P.A. Lee, S. Uchida, H. Eisaki, G.S. Boebinger, Y. Ando, Y.S. Lee, M.A. Kastner, R.J. Birgeneau, N.J. Curro, P.C. Hammel, J. Zaanen, H. Brom, J. Haase, and C.P. Slichter among others. This work was financially supported by NSF Grant Nos. DMR-9971264 and DMR 98-08941 through the MRSEC program.

[1] For recent theoretical discussions, see A. H. Castro Neto and D. Hone, Phys. Rev. Lett. **76**, 2165 (1996); C. N. A. van Duin and J. Zaanen, *ibid.* **80**, 1513 (1998); S. R. White and D. J. Scalapino, *ibid.* **80**, 1272 (1998); S. A. Kivelson, E. Fradkin, and V. J. Emery, Nature (London) **393**, 550 (1998); M. Vojta and S. Sachdev, Phys. Rev. Lett. **83**, 3916 (1999); L. P. Pryadko, S. A. Kivelson, V. J. Emery, Y. B. Bazaliy, and E. A. Demler, Phys. Rev. B **60**, 7541 (1999). For earlier theoretical works see J. Zannen and O. Gunnarsson, *ibid.* **40**, 7391 (1989); D. Poiblanc and T. M. Rice, *ibid.* **39**, 9749 (1989); K. Machida, Physica C **158**, 192 (1989); V. J. Emery, S. A. Kivelson, and H.-Q. Lin, Phys. Rev. Lett. **64**, 475 (1990); and C. Castellani, C. Di Castro, and M. Grilli, *ibid.* **75**, 4650 (1995).

[2] J. M. Tranquada, B. J. Sternlieb, J. D. Axe, Y. Nakamura, and S. Uchida, Nature (London) **375**, 561 (1995).

[3] T. Suzuki, T. Goto, K. Chiba, T. Shinoda, T. Fukase, H. Kimura, K. Yamada, M. Ohashi, and Y. Yamaguchi, Phys. Rev. B **57**, R3229 (1998).

[4] H. Kimura, H. Hirota, H. Matsushita, K. Yamada, Y. Endoh, S.-H. Lee, C. F. Majkrzak, R. Erwin, G. Shirane, M. Greven, Y. S. Lee, M. A. Kastner, and R. J. Birgeneau, Phys. Rev. B **59**, 6517 (1999).

[5] S. Wakimoto, G. Shirane, Y. Endoh, K. Hirota, S. Ueka, K. Yamada, R. J. Birgeneau, M. A. Kastner, Y. S. Lee, P. M. Gehring, and S.-H. Lee, Phys. Rev. B **60**, R769 (1999).

[6] Y. S. Lee, R. J. Birgeneau, M. A. Kastner, Y. Endoh, S. Wakimoto, K. Yamada, R. W. Erwin, S.-H. Lee, and G. Shirane, Phys. Rev. B **60**, 3643 (1999).

[7] J. M. Tranquada, J. D. Axe, N. Ichikawa, Y. Nakamura, S. Uchida, and B. Nachumi, Phys. Rev. B **54**, 7489 (1996).

[8] J. M. Tranquada, J. D. Axe, N. Ichikawa, A. R. Moodenbaugh, Y. Nakamura, and S. Uchida, Phys. Rev. Lett. **78**, 338 (1997).

[9] J. M. Tranquada, N. Ichikawa, and S. Uchida, Phys. Rev. B **59**, 14 712 (1999).

[10] A. W. Hunt, P. M. Singer, K. R. Thurber, and T. Imai, Phys. Rev. Lett. **82**, 4300 (1999).

[11] P. M. Singer, A. W. Hunt, A. F. Cederström, and T. Imai, Phys. Rev. B **60**, 15 345 (1999).

[12] N. J. Curro, P. C. Hammel, B. J. Suh, M. Hücker, B. Búcher, U. Ammerahl, and A. Revcolevscji, Phys. Rev. Lett. **85**, 642 (2000).

[13] G. B. Teitel'baum, B. Büchner, and H. de Gronckel, Phys. Rev. Lett. **84**, 2949 (2000).

[14] M.-H. Julien, A. Campana, A. Rigamonti, P. Carretta, F. Borsa, P. Kuhns, A. P. Reyes, W. G. Moulton, M. Horvatić, C. Berthier, A. Vietkin, and A. Revcolevschi, Phys. Rev. B **63**, 144508 (2001).

[15] B. Rameev, E. Kukovitskii, V. Kataev, and G. Teitel'baum, Physica C **246**, 309 (1995).

[16] V. Kataev, B. Rameev, A. Validov, B. Büchner, M. Hücher, and R. Borowski, Phys. Rev. B **58**, R11 876 (1998).

[17] M.v. Zimmermann, A. Vigliante, T. Niemöller, N. Ichikawa, T. Frello, J. Madsen, P. Wochner, S. Uchida, N. H. Andersen, J. M. Tranquada, D. Gibbs, and J. R. Schneider, Europhys. Lett. **41**, 629 (1998).

[18] T. Niemöller, H. Hünnefeld, J. R. Schneider, N. Ichikawa, S. Uchida, T. Frello, N. H. Andersen, and J. M. Tranquada, Eur. Phys. J. B **12**, 509 (1999).

[19] Y. Ando, G. S. Boebinger, A. Passner, T. Kimura, and K. Kishio, Phys. Rev. Lett. **75**, 4662 (1995).

[20] G. S. Boebinger, Yoichi Ando, A. Passner, T. Kimura, M. Okuya, J. Shimoyama, K. Kishio, K. Tamasaku, N. Ichikawa, and S. Uchida, Phys. Rev. Lett. **77**, 5417 (1996).

[21] T. Noda, H. Eisaki, and S. Uchida, Science **286**, 265 (1999).

[22] N. Ichikawa, S. Uchida, J. M. Tranquada, T. Niemoeller, P. M. Gehring, S.-H. Lee, and J. R. Schneider, Phys. Rev. Lett. **85**, 1738 (2000).

[23] S. Uchida, N. Ichikawa, T. Noda, and H. Eisaki, in *Physics and Chemistry of Transition Metal Oxides*, edited by H. Fukuyama and N. Nagaosa, Vol. 125 of Springer Series in Solid State Sciences (Springer, New York, 1999).

[24] N. Ichikawa, S. Uchida, J. M. Tranquada, T. Niemöller, P.M. Gehring, S.-H. Lee, and J. R. Schneider (unpublished); N. Ichikawa, Ph.D. thesis, University of Tokyo, 1999.

[25] A. Ino, T. Mizokawa, K. Kobayashi, A. Fujimori, T. Sasagawa, T. Kimura, K. Kishio, K. Tamasaku, H. Eisaki, and S. Uchida, Phys. Rev. Lett. **81**, 2124 (1998).

[26] X. J. Zhou, P. Bogdanov, S. A. Keller, T. Noda, H. Eisaki, S. Uchida, Z. Hussain, and Z.-X. Shen, Science **286**, 268 (1999).

[27] G. M. Luke, L. P. Le, B. J. Strenlieb, W. D. Wu, Y. J. Uemura, J. H. Brewer, T. M. Riseman, and S. Ishibashi, Physica C **185-189**, 1175 (1991).
[28] K.-I. Kumagi, K. Kawano, I. Watanabe, K. Nishiyama, and K. Nagamine, Hyperfine Interact. **86**, 473 (1994).
[29] B. Nachumi, Y. Fudamoto, A. Keren, K. M. Kojima, M. Larkin, G. M. Luke, J. Merrin, O. Tchernyshyov, Y. J. Uemura, N. Ichikawa, M. Goto, H. Takagi, S. Uchida, M. K. Crawford, E. M. McCarron, D. E. MacLaughlin, and R. H. Heffner, Phys. Rev. B **58**, 8760 (1998).
[30] Ch. Niedermayer, C. Bernhard, T. Blasius, A. Golnik, A. Moodenbaugh, and J. I. Budnick, Phys. Rev. Lett. **80**, 3843 (1998).
[31] K. M. Kojima, H. Eisaki, S. Uchida, Y. Fudamoto, I. M. Gat, A. Kinkhabwala, M. I. Larkin, G. M. Luke, and Y. J. Uemura, Physica B **289-290**, 343 (2000).
[32] A. T. Savici, Y. Fudamoto, I. M. Gat, M. I. Larkin, Y. J. Uemura, G. M. Luke, K. M. Kojima, Y. S. Lee, M. A. Kastner, and R. J. Birgeneau, Physica B **289-290**, 338 (2000).
[33] T. Imai, K. Yoshimura, T. Uemura, H. Yasuoka, and K. Kosuge, J. Phys. Soc. Jpn. **59**, 3846 (1990).
[34] K. Yoshimura, T. Uemura, M. Kato, T. Shibata, K. Kosuge, T. Imai, and H. Yasuoka, in *The Physics and Chemistry of Oxide Superconductors*, edited by Y. Iye and H. Yasuoka (Springer-Verlag, Berlin, 1992), pp. 405–407.
[35] H. Tou, M. Matsumura, and H. Yamagata, J. Phys. Soc. Jpn. **61**, 1477 (1992).
[36] J. H. Cho, F. Borsa, D. C. Johnston, and D. R. Torgenson, Phys. Rev. B **46**, 3179 (1992).
[37] F. C. Chou, F. Borsa, J. H. Cho, D. C. Johnston, A. Lascialfari, D. R. Torgeson, and J. Ziolo, Phys. Rev. Lett. **71**, 2323 (1993).
[38] T. Goto, S. Kazama, K. Miyagawa, and T. Fukase, J. Phys. Soc. Jpn. **63**, 3494 (1994).
[39] S. Ohsugi, Y. Kitaoka, H. Yamanaka, K. Ishida, and K. Asayama, J. Phys. Soc. Jpn. **63**, 2057 (1994).
[40] S. Ohsugi, J. Phys. Soc. Jpn. **64**, 3656 (1995).
[41] A. Abragam, *Principles of Nuclear Magnetism* (Oxford University Press, New York, 1978).
[42] C. P. Slichter, *Principles of Magnetic Resonance*, 3rd ed. (Springer-Verlag, New York, 1989).
[43] B. Keimer, N. Belk, R. J. Birgeneau, A. Cassanho, C. Y. Chen, M. Greven, M. A. Kastner, A. Aharony, Y. Endoh, R. W. Erwin, and G. Shirane, Phys. Rev. B **46**, 14 034 (1992).
[44] B. J. Sternlieb, M. Sato, S. Shamoto, G. Shirane, and J. M. Tranquada, Phys. Rev. B **47**, 5320 (1993).
[45] G. Aeppli, T. E. Mason, S. M. Hayden, H. A. Mook, and J. Kulda, Science **278**, 1432 (1997).
[46] M. Breuer, B. Büchner, R. Müller, M. Cramm, O. Maldonado, A. Freimuth, B. Roden, R. Borowski, B. Heymer, and D. Wohlleben, Physica C **208**, 217 (1993).
[47] B. Büchner, M. Breuer, M. Cramm, A. Freimuth, H. Micklitz, W. Schlabitz, and A. P. Kampf, J. Low Temp. Phys. **95**, 285 (1994).
[48] H. Yasuoka, J. Phys. Soc. Jpn. **19**, 1182 (1964).
[49] P. Heller and G. Benedek, Phys. Rev. Lett. **8**, 428 (1962).
[50] T. Tsuda, T. Shimizu, H. Yasuoka, K. Kishio, and K. Kitazawa, J. Phys. Soc. Jpn. **57**, 2908 (1988).
[51] H. Yasuoka, T. Shimizu, Y. Ueda, and K. Kosuge, J. Phys. Soc. Jpn. **57**, 2659 (1988).
[52] D. E. MacLaughlin, J. P. Vithayathil, H. B. Brom, J. C. J. M. de Rooy, P. C. Hammel, P. C. Canfield, A. P. Reyes, Z. Fisk, J. D. Thomson, and S-W. Cheong, Phys. Rev. Lett. **72**, 760 (1994).
[53] A. Lombardi, M. Mali, J. Roos, and D. Brinkman, Phys. Rev. B **54**, 93 (1996).
[54] F. Mila and T. M. Rice, Physica C **157**, 561 (1988).
[55] D. Vaknin, S. K. Sinha, D. E. Moncton, D. C. Johnston, J. M. Newsam, C. R. Safinya, and H. E. King, Jr., Phys. Rev. Lett. **58**, 2802 (1987).
[56] T. Imai, C. P. Slichter, K. Yoshimura, and K. Kosuge, Phys. Rev. Lett. **70**, 1002 (1993).
[57] Y. J. Uemura, W. J. Kossler, X. H. Yu, J. R. Kempton, H. E. Shone, D. Opie, C. E. Stronach, D. C. Johnson, M. S. Alverez, and D. P. Goshorn, Phys. Rev. Lett. **59**, 1045 (1987); S. Uchida, Physica C **185-189**, 1175 (1991).
[58] K. Yoshimura, T. Imai, T. Shimizu, Y. Ueda, K. Kosuge, and H. Yasuoka, J. Phys. Soc. Jpn. **58**, 3057 (1989).
[59] K. Yoshimura, T. Uemura, M. Kato, K. Kosuge, T. Imai, and H. Yasuoka, Hyperfine Interact. **79**, 876 (1993).
[60] Unpublished ^{63}Cu NQR spectra observed for $x=0.02$, 0.04, 0.075, and 0.15 in $La_{2-x}Sr_xCuO_4$ measured up to 800 K for Imai *et al.* (Ref. 56).
[61] S. Kambe, H. Yasuoka, H. Takagi, S. Uchida, and Y. Tokura, J. Phys. Soc. Jpn. **60**, 400 (1991).
[62] H. Nishihara, H. Yasuoka, T. Shimizu, T. Tsuda, T. Imai, S. Sasaki, S. Kanbe, K. Kishio, K. Kitazawa, and K. Fueki, J. Phys. Soc. Jpn. **56**, 4559 (1987).
[63] Y. Kitaoka, S. Hiramatsu, K. Ishida, T. Kohara, and K. Asayama, J. Phys. Soc. Jpn. **56**, 3024 (1987).
[64] G. M. Muha, J. Magn. Reson. **53**, 85 (1983).
[65] R. Kubo and T. Toyabe, in the *Proceedings of Colloque Ampere XIV*, edited by R. Blinc (North-Holland, Amsterdam, 1967), p. 810.
[66] Y. J. Uemura, T. Yamazaki, R. S. Hayano, R. Nakai, and C. Y. Huang, Phys. Rev. Lett. **45**, 583 (1980).
[67] E. Vavilova, E. Kukovitskij, and G. B. Teitel'baum, Physica B **280**, 205 (2000).
[68] G. B. Teitel'baum, I. M. Abu-Shiekah, O. Bakharev, H. B. Brom, and J. Zaanen, Phys. Rev. B **63**, 020507 (2001).
[69] B. J. Suh, P. C. Hammel, M. Hücker, B. Büchner, U. Ammerahl, and A. Revcolevschi, Phys. Rev. B **61**, R9265 (2000).
[70] K. Yamada, C. H. Lee, K. Kurahashi, J. Wada, S. Wakimoto, S. Ueki, H. Kimura, Y. Endoh, S. Hosoya, G. Shirane, R. J. Birgeneau, M. Greven, and M. A. Kastner, Phys. Rev. B **57**, 6165 (1998).
[71] Note that the contours plotted in Figs. 10 and 14(b) represent the function $fD(T,f)$ where the extra factor of f arises from $\int D(T,f)df=\int fD(T,f)d(\log f)$. Plotting $fD(T,f)$ allows direct integration in $d(\log f)$. Similarly, in Figs. 12 and 14a the distribution of T_1 is plotted with a multiplicative factor of T_1 so that it can be easily integrated by eye. The distribution is actually a Gaussian in $\log T_1$ divided by T_1.
[72] K. R. Thurber, T. Imai, T. Saito, M. Azuma, M. Takano, and F. C. Chou, Phys. Rev. Lett. **84**, 558 (2000).
[73] T. Imai, C. P. Slichter, K. Yoshimura, M. Katoh, and K. Kosuge, Phys. Rev. Lett. **71**, 1254 (1993).
[74] S. M. Hayden, G. Aeppli, R. Osborn, A. D. Taylor, T. G. Perring, S.-W. Cheong, and Z. Fisk, Phys. Rev. Lett. **67**, 3622 (1991).
[75] R. R. P. Singh, P. A. Fleury, K. B. Lyons, and P. E. Sulewski, Phys. Rev. Lett. **62**, 2736 (1989).
[76] Y. J. Kim, R. J. Birgeneau, M. A. Kastner, Y. S. Lee, Y. Endoh,

G. Shirane, and K. Yamada, Phys. Rev. B **60**, 3294 (1999).
[77] B. J. Suh, P. C. Hammel, Y. Yoshinari, J. D. Thompson, J. L. Sarrao, and Z. Fisk, Phys. Rev. Lett. **81**, 2791 (1998).
[78] T. Moriya, Prog. Theor. Phys. **16**, 23 (1956).
[79] S. Chakravarty and R. Orbach, Phys. Rev. Lett. **64**, 224 (1990).
[80] T. Moriya, Prog. Theor. Physics (Kyoto) **16**, 641 (1956).
[81] In our earlier publications (Refs. 10 and 11) we did not distinguish between T_{NQR} and T_{charge}. However, recent scattering measurements by Ichikawa *et al.* (Ref. 22) showed that the onset of ^{63}Cu NQR wipeout precedes the onset of charge order with short-range spatial coherence at T_{charge} for $x<0.12$. Accordingly, we identify the onset of wipeout as T_{NQR} hereafter. This is the same notation which we originally used in the initial version of Hunt *et al.* (Ref. 10) [see cond-mat/9902348 (unpublished)]. We eliminated many new symbols including T_{NQR}, assuming that $T_{NQR}=T_{charge}$ for all concentrations.
[82] I. M. Abu-Shiekah, O. O. Bernal, A. A. Menovsky, H. Brom, and J. Zaanen, Phys. Rev. Lett. **83**, 3309 (1999).
[83] The ^{139}La NMR wipeout observed by Abu-Shiekah *et al.* (Ref. 82) below 200 K in $La_2NiO_{4+\delta}$ is not necessarily caused directly by charge fluctuations by themselves, though the temperature dependence of the wipeout fraction tracks the charge order parameter measured by neutron scattering quite well. Because of the strong hybridization of the ^{139}La atomic orbitals to Ni spin with a $3d^8$ configuration, the magnetic hyperfine interaction between Ni and La is sizable. This means that if Ni *d*-spin fluctuations slow down below charge ordering, ^{139}La NMR signal can be wiped out by the *indirect*, slowing spin mechanism caused by charge order. This scenario is particularly plausible for $La_2NiO_{4+\delta}$ because the application of a high magnetic field to detect NMR is known to cause an extra slowing down of spins (Ref. 85).
[84] J. M. Tranquada, P. Wochner, A. R. Moodenbaugh, and D. J. Buttrey, Phys. Rev. B **55**, R6113 (1997).
[85] P. Wochner, J. M. Tranquada, D. J. Buttrey, and V. Sachan, Phys. Rev. B **57**, 1066 (1998).
[86] P. Butaud, P. Ségaransan, C. Berthier, J. Dumas, and C. Shlenker, Phys. Rev. Lett. **55**, 253 (1985).
[87] J. H. Ross, Jr., Z. Wang, and C. P. Slichter, Phys. Rev. Lett. **56**, 663 (1986).
[88] K. Nomura, T. Sambongi, K. Kume, and M. Sato, Physica B **143**, 117 (1986).
[89] D. E. MacLaughling and H. Alloul, Phys. Rev. Lett. **36**, 1158 (1976).
[90] H. Nagasawa and W. A. Steyert, J. Phys. Soc. Jpn. **28**, 1171 (1970).
[91] F. Borsa, M. Corti, T. Goto, A. Rigamonti, D. C. Johnston, and F. C. Chou, Phys. Rev. B **45**, 5756 (1992).
[92] S. M. Hayden, G. Aeppli, H. A. Mook, T. G. Perring, T. E. Mason, S.-W. Cheong, and Z. Fisk, Phys. Rev. Lett. **76**, 1344 (1996).
[93] D. C. Johnston, Phys. Rev. Lett. **62**, 957 (1989).
[94] H. Y. Hwang, B. Batlogg, H. Takagi, H. L. Kao, R. J. Cava, J. J. Krajewski, and W. F. Peck, Jr., Phys. Rev. Lett. **72**, 2636 (1994).
[95] M. C. Chen and C. P. Slichter, Phys. Rev. B **27**, 278 (1983).
[96] A. P. Murani, J. Magn. Magn. Mater. **22**, 271 (1981).
[97] M. Sera, Y. Ando, S. Kondoh, K. Fukuda, M. Sato, I. Watanabe, S. Nakashima, and K. Kumagai, Solid State Commun. **69**, 851 (1989).
[98] S. Ikegawa, T. Yamashita, T. Sakurai, R. Itti, H. Yamauchi, and S. Tanaka, Phys. Rev. B **43**, 2885 (1991).
[99] T. Imai (unpublished).
[100] G. Q. Zheng, Y. Kitaoka, Y. Oda, and K. Asayama, J. Phys. Soc. Jpn. **58**, 1910 (1989).
[101] M. Itoh, K. Karashima, M. Kyogaku, and I. Aoki, Physica C **160**, 177 (1989).
[102] P. M. Singer, A. W. Hunt, T. Imai, N. Ichikawa, and S. Uchida (unpublished).
[103] J. Haase, C. P. Slichter, R. Stern, C. T. Milling, and D. G. Hinks, Physica C **341**, 1727 (2000).
[104] S. Fujiyama, Y. Itoh, H. Yasuoka, and Y. Ueda, J. Phys. Soc. Jpn. **66**, 2864 (1997).
[105] H. Hiraka, Y. Endoh, M. Fujita, Y. S. Lee, J. Kulda, A. Ivanov, and R. J. Birgeneau, J. Phys. Soc. Jpn. **70**, 853 (2001).
[106] We recall the presence of an enhanced Lorentzian $^{63}1/T_2$ near T_{NQR} due to magnetic fluctuations (Refs. 10 and 11). We also recall the possibility of contributions from *direct* charge contributions to relaxation and wipeout (Refs. 10 and 11).